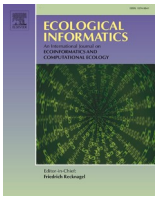
Ecological Informatics 99 (2026) 104113



Contents lists available at ScienceDirect

Ecological Informatics

journal homepage: www.elsevier.com/locate/ecolinf



Rarefaction profiles for repeated biodiversity surveys: integrating temporal variability and trend along sample-based accumulation curves

Giovanni Bacaro [a,*], Emanuele Fanfarillo [b], Simona Maccherini [b]

[a] Department of Life Sciences, University of Trieste, Via L. Giorgieri 10, Trieste, 34127, Italy
[b] Department of Life Sciences, University of Siena, Via Mattioli 4, Siena, 53100, Italy

ARTICLE INFO

Keywords:
Alpha diversity
Biodiversity monitoring
Functional diversity
Gamma diversity
Sample-based rarefaction
Temporal variability

ABSTRACT

Repeated biodiversity surveys are often summarised by one diversity value per survey date, although temporal change may be expressed differently at the scale of individual sampling units, across the full sampled community, or along the accumulation process linking the two. We introduce rarefaction profiles for repeated biodiversity surveys, based on sample-based rarefaction applied independently to repeated survey dates. For each survey date, a rarefaction curve is calculated by accumulating comparable sampling units. Temporal variability and temporal trend are then estimated at each accumulation level m, from $m = 1$, representing the expected diversity of one sampling unit, to $m = N$, representing sampled gamma diversity within the defined sampling focus. The approach is metric-general and can be applied to taxonomic diversity, functional diversity and directional community descriptors, provided that the target quantity can be calculated for pooled subsets of sampling units. We provide a reproducible *R* implementation that returns survey-specific rarefaction curves, temporal variability profiles, temporal trend profiles, alpha- and sampled-gamma summaries, whole-profile summaries and contrasts among groups. We illustrate the method using data from 16 vegetation surveys conducted between 2001 and 2019 at the Monte Labbro long-term grassland experiment in southern Tuscany, Italy. Ungrazed plots showed higher temporal variability and stronger negative temporal change in richness and Shannon diversity than grazed plots, with resampling-based uncertainty supporting these taxonomic contrasts across most or all of the accumulation gradient. Exact within-block label randomisation showed that the taxonomic Grazed–Ungrazed contrasts were stronger than expected under random treatment assignment across the complete accumulation profile, whereas a species-allocation null model indicated non-random accumulation-dependent richness structure primarily in ungrazed plots. Functional responses differed from taxonomic responses: point estimates indicated higher temporal variability of functional richness in grazed plots and higher temporal variability and an increasing temporal trend in community-weighted mean trait displacement in ungrazed plots, but sampling uncertainty around these functional treatment contrasts was substantially greater. An alternative permanent-plot bootstrap produced the same overall uncertainty pattern. Rarefaction profiles for repeated biodiversity surveys therefore provide a reproducible way to analyse where, along sample-based accumulation curves, biodiversity change is variable, directional or both.

1. Introduction

Biodiversity change is intrinsically scale dependent. This is a general problem in ecology, because ecological patterns detected at one grain or extent do not necessarily translate to another (Chase et al., 2018; Levin, 1992). In long-term community data, alpha diversity can fluctuate strongly among years while sampled gamma diversity for the defined sampling focus remains comparatively stable. When plot-level dynamics are asynchronous, increases in some sampling units may offset decreases in others as units are pooled, producing spatial compensation and attenuating temporal variation at the sampled-gamma endpoint. The opposite pattern is also possible: mean plot-level alpha diversity may remain stable while species gains, losses or redistribution change species occupancy and among-unit complementarity; these changes may modify the accumulation curve and, when they affect the cumulative species pool, sampled gamma diversity. These mechanisms are not identified by the rarefaction profile alone, but they explain why local and cumulative temporal signals need not coincide. In both cases, the relationship

* Corresponding author.
E-mail address: gbacaro@units.it (G. Bacaro).

https://doi.org/10.1016/j.ecoinf.2026.104113
Received 26 June 2026; Received in revised form 20 October 2026; Accepted 20 October 2026
Available online 21 October 2026
1574-9541/© 2026 The Author(s). Published by Elsevier B.V. This is an open access article under the CC BY license (http://creativecommons.org/licenses/by/4.0/).

between alpha and sampled gamma diversity carries information on the spatial organisation of diversity and on beta-related differences among sampling units. This creates a persistent difficulty for long-term biodiversity monitoring, where each survey year is often reduced to a single value of richness, diversity or composition. Such summaries can be informative, but they do not show whether temporal change is mainly expressed in alpha diversity, in sampled gamma diversity, or in the change from local to cumulative diversity as sampling units are progressively pooled (Bacaro et al., 2009; Yoccoz et al., 2001).

This limitation is well recognised in the biodiversity-change literature. Large syntheses of assemblage change have shown that local species richness can remain nearly stable even when species composition is reorganised through time (Dornelas et al., 2014). At broader scales, the magnitude and direction of biodiversity change also vary among ecosystems, regions and taxonomic groups (Blowes et al., 2019). These results explain why temporal change cannot be evaluated from richness alone and why compositional turnover has become central in biodiversity monitoring. This has motivated increasing attention to temporal beta diversity, because changes in species identity, abundance structure and compositional turnover can be more informative than changes in species number alone (Hillebrand et al., 2018; Magurran et al., 2019; Shimadzu et al., 2015). The same limitation becomes even more evident when biodiversity change is interpreted functionally: species richness does not necessarily capture shifts in trait composition, ecological strategies or ecosystem-functioning potential (Carmona et al., 2016; Lavorel and Garnier, 2002; McGill et al., 2006; Violle et al., 2007). For long-term monitoring, this means that a single annual diversity value may be insufficient to describe the structure of biodiversity change and may provide only a partial description of the sampled assemblage (Bacaro, 2026). Richness, composition and functional structure may differ between the observational grain of individual sampling units and the cumulative community represented by the full sampling focus: changes in plot-level diversity do not necessarily imply changes in the cumulative sampled community, and changes in the cumulative community may occur even when average plot-level diversity appears stable. Observed spatial or temporal differences may also arise from imperfect detection rather than genuine changes in species occurrence. Detectability can vary with phenology or life-history stage, population density, survey effort, observer and survey timing, producing apparent absences in both animal inventories and long-term plant monitoring (Alexander et al., 2009; Bacaro and Fonda, 2026; Watson, 2010). Unless detectability is modelled separately, profiles based on recorded occurrences do not distinguish changes in true occurrence from changes in detection.

Rarefaction is directly relevant to this issue because it describes how diversity changes as sampling units are progressively accumulated. Classical sample-based rarefaction and species accumulation curves were developed to compare assemblages under unequal sampling effort or different levels of sample completeness (Colwell et al., 2004; Gotelli and Colwell, 2001). This logic was later generalised in the Hill-number framework, where richness, exponential Shannon diversity and inverse Simpson diversity can be compared after standardising either sample size or sample coverage (Chao et al., 2014; Chao and Jost, 2012). In most applications, rarefaction is used to compare assemblages at a common sampling effort or sample coverage. This endpoint comparison is useful, but it uses only one point of the curve. The rest of the curve describes how diversity increases as sampling units are added. It therefore shows how plot-level diversity is progressively integrated into the cumulative diversity of the sampled community, and it provides information on the contribution of differences among sampling units to the alpha–gamma relationship. This broader use of rarefaction is already present in several extensions of the method. Spatially constrained rarefaction was developed to account for the fact that nearby sampling units may contain similar communities and should not always be treated as freely exchangeable (Bacaro et al., 2016; Chiarucci et al., 2008, 2009). Functional rarefaction applies the same sample-based logic to trait-based diversity measures, allowing functional diversity to be compared under standardised sampling conditions (Ricotta et al., 2012). Related approaches have extended rarefaction to functional and phylogenetic resemblance among communities (Pavoine, 2020; Pavoine and Ricotta, 2014), to beta diversity and multiple-site dissimilarity (Ricotta et al., 2019), and, more recently, to Hill-number beta-diversity standardisation through the *iNEXT.beta3D* framework (Chao et al., 2023). The *Rarefy R* package brings several of these developments into a common computational framework by implementing sample-based, spatially explicit rarefaction for taxonomic, functional, phylogenetic and user-defined diversity metrics (Thouverai et al., 2026). These developments indicate that rarefaction can be used not only to standardise richness, but also to examine how different dimensions of biodiversity change as sampling units are accumulated. The temporal extension proposed here follows the same logic. Rather than reducing each survey occasion to a single standardised diversity value, it compares rarefaction curves calculated independently for repeated survey occasions. Differences among these curves at each accumulation level indicate whether temporal variability is strongest at the alpha-diversity endpoint, at the sampled-gamma endpoint, or at intermediate accumulation levels.

The temporal dimension of biodiversity scaling has usually been addressed through species-time and species-time-area relationships, which ask how richness increases as temporal duration, spatial extent or both are expanded (Adler et al., 2005; Adler and Lauenroth, 2003; Preston, 1960; Rosenzweig, 1995; White et al., 2006). These approaches quantify biodiversity accumulation over increasing temporal or spatio-temporal extent. The framework developed here asks a different question. When the same sampling units are surveyed repeatedly through time, do changes in diversity appear at the level of individual sampling units, in the cumulative community sampled by all units, or along the accumulation process as increasing numbers of units are pooled? Importantly, the accumulation level m represents the number of pooled sampling units and does not, by itself, define a spatial grain, spatial extent or contiguous sampled area. Because $m = 1$ retains the observational grain of an individual sampling unit and $m = N$ represents the complete sampled focus, the profile can nevertheless show whether temporal differences are stronger at either endpoint or change systematically with aggregation. Different profile shapes may be consistent with processes such as local fluctuations, asynchronous dynamics among sampling units, changes in spatially restricted species or increasing among-unit differentiation. However, these are possible and non-exclusive ecological interpretations rather than processes that can be inferred directly from unconstrained sample-based rarefaction. Their interpretation depends on the spatial arrangement and separation of sampling units, habitat composition and spatial dependence, and therefore requires independent ecological or spatial information (Bacaro et al., 2016; Chiarucci et al., 2009). The proposed repeated-survey rarefaction profiles therefore do not measure richness accumulation through time, as species–time relationships do. They measure how the rarefaction curve itself varies among survey years, allowing temporal change to be interpreted along a sampling-unit accumulation gradient.

Here, we formalise rarefaction profiles for repeated biodiversity surveys as an accumulation-explicit framework based on temporally repeated sample-based rarefaction. In this framework, alpha, beta and gamma diversity are interpreted with reference to the sampling design. The individual sampling unit defines the observational grain and therefore the alpha-diversity endpoint. The full set of sampling units included in a given survey defines the sampled focus, and diversity calculated after pooling all those units represents sampled gamma diversity for that focus. Intermediate values along the accumulation curve are beta-relevant because they describe how differences among sampling units modify the transition from local diversity to cumulative diversity. However, intermediate values of m represent levels of sampling-unit accumulation or aggregation, not a sequence of increasingly large spatial grains or extents. Under this interpretation, gamma diversity is not treated as an absolute property of a landscape, but as the cumulative diversity of the defined set of sampling units. If the number or spatial

extent of sampling units changes, the sampled gamma endpoint of the analysis changes accordingly.

For each survey date, the method calculates a rarefaction curve from the available sampling units and compares these curves along equivalent values of accumulated sampling units m. We focus on two complementary outputs. The first is a temporal variability profile, which measures how strongly rarefied diversity varies among survey dates at each value of m. The second is a temporal trend profile, which estimates the direction and magnitude of change through time at the same positions along the accumulation curve. At $m = 1$, the profiles describe change at the expected alpha-diversity scale; at $m = N$, they describe change at the sampled-gamma scale; intermediate values show how variability and trend change as sampling units are progressively pooled. The approach can be applied to taxonomic diversity, functional diversity and directional functional displacement, provided that the metric can be calculated for pooled subsets of sampling units.

The framework distinguishes diagnostic patterns of temporal diversity change by combining the shape of survey-specific rarefaction curves, the temporal variability profile and, when relevant, the temporal trend profile. The main idealised patterns and their possible ecological interpretations are developed in the Conceptual framework below, where they are treated as diagnostic and non-exclusive rather than as direct evidence of particular ecological processes.

We develop the framework in two steps. First, idealised examples are used to define the main temporal diversity patterns expected along the alpha–gamma accumulation gradient and to provide a conceptual reference for interpreting empirical profiles. Second, the framework is applied to data from 16 vegetation surveys conducted between 2001 and 2019 at the Monte Labbro long-term grassland experiment in southern Tuscany, Italy, previously analysed by Pavanetto et al. (2025). The worked example compares grazed and ungrazed permanent plots and evaluates both temporal variability and directional change in taxonomic and functional diversity. Specifically, we ask whether richness, Shannon diversity, functional richness and community-weighted mean trait displacement show consistent responses along the accumulation curve, or whether alpha-scale and sampled-gamma-scale summaries support different ecological interpretations.

2. Conceptual framework

2.1. Method at a glance

The method requires repeated observations of comparable sampling units. The analysis-ready data must identify the survey occasion, the sampling-unit identifier and, where relevant, the group or treatment, together with the species incidence or abundance data—or the corresponding information required to calculate another target metric—for each sampling unit. Functional applications additionally require a harmonised trait table. The workflow comprises six steps: (1) within each survey occasion and group, subsets of $m = 1, \ldots, N$ sampling units are pooled; (2) the target metric is calculated for every subset, or for a reproducible random sample of subsets when complete enumeration is impractical, and averaged to obtain the survey-specific rarefaction curve; (3) survey-specific curves are aligned at equivalent values of m, and temporal variability and temporal change are estimated across survey occasions at each m, using the actual survey dates; (4) when the number of available sampling units differs among occasions or groups, comparisons are restricted to a common range of m, or alternatively standardised by sample coverage or analysed using a prespecified resampling scheme; (5) the principal outputs are the survey-specific rarefaction curves and intervals, temporal-variability and temporal-change profiles, alpha and sampled-gamma endpoints, whole-profile summaries and, where relevant, group contrasts with uncertainty estimates; and (6) profile shape is interpreted by asking whether temporal differences are attenuated, emerge or persist as sampling units are accumulated. These profiles describe where along the accumulation gradient the temporal signal occurs; they do not by themselves identify temporal synchrony, spatial compensation or other ecological mechanisms. Fig. 1 summarises this sequence graphically, while the formal definitions and implementation details are provided below.

Consider a community surveyed at T time steps with N comparable sampling units at each time step. In the simplest case, sampling units are permanent plots surveyed with the same protocol through time. The sampling unit defines the grain of observation and therefore the alpha endpoint of the analysis, while the full set of N units defines the sampled focus over which gamma diversity is evaluated (Scheiner et al., 2011; Tuomisto, 2010a, 2010b; Whittaker, 1960). The accumulation of diversity between the alpha and gamma endpoints depends on how similar or different the sampling units are in composition. For metrics such as species richness and convex-hull functional richness, the contribution of new species or trait combinations generally increases the expected accumulated value. Other metrics, including functional dispersion and *CWM* displacement, may exhibit non-monotonic accumulation patterns, which should be interpreted according to the properties of the selected metric. The intermediate portion of the curve therefore provides information on the contribution of among-unit heterogeneity to the sampled community, a central component of alpha–beta–gamma diversity relationships. Importantly, m is an accumulation index: it denotes the number of sampling units pooled in the calculation of expected diversity. Because standard sample-based rarefaction draws subsets without constraining their spatial configuration, increasing m does not correspond to an increase in a uniquely defined spatial grain, extent or contiguous area. Two subsets with the same m may have very different spatial configurations. Intermediate values of m should therefore be interpreted as aggregation levels, whereas any explicit spatial interpretation depends on plot size, plot separation, habitat composition and spatial dependence among sampling units. When these properties are central to the ecological question, spatially constrained rarefaction can be used to incorporate them directly (Bacaro et al., 2016; Chiarucci et al., 2009). This interpretation depends on the sampling design, because grain, focus and extent determine whether a diversity value is best understood as local, cumulative or extrapolated diversity (Scheiner, 2003; Scheiner et al., 2011). Accordingly, $m = N$ should be interpreted as the gamma-diversity endpoint of the defined sampling focus, not as an estimate of regional or landscape gamma diversity unless the sampling design was explicitly constructed for that purpose. If additional sampling units are included, the same numerical value of m becomes an intermediate point of a longer accumulation curve rather than the sampled-gamma endpoint.

For any diversity metric D, a sample-based rarefaction curve at time t can be written as the expected value of D after pooling m sampling units drawn without replacement from the N units available at that time:

$$R_{D,t}(m) = E\left[D\left(X_{t,m}\right)\right] \quad (1)$$

where $X_{t,m}$ is a subset of m sampling units from time t. When D is species richness, this is the usual sample-based taxonomic rarefaction curve, following the logic of rarefying assemblages to a common number of sampling units (Colwell et al., 2004; Gotelli and Colwell, 2001). When D is a Hill-number diversity measure, the same formulation can be used for richness, exponential Shannon diversity or inverse Simpson diversity, with interpretation depending on the order of diversity considered (Chao et al., 2014; Chao and Jost, 2012). The same formulation can be used for functional descriptors, provided that the metric can be calculated after pooling a subset of sampling units. Functional diversity metrics summarise different properties of community trait structure, including pairwise trait dissimilarity, dispersion around a functional centroid and the amount of occupied trait space (Laliberté and Legendre, 2010; Mason et al., 2005; McGill et al., 2006; Villéger et al., 2008). For example, Rao's quadratic entropy, functional dispersion and convex-hull functional richness can be rarefied in the same sample-based way as taxonomic diversity, so that the curve describes how the expected

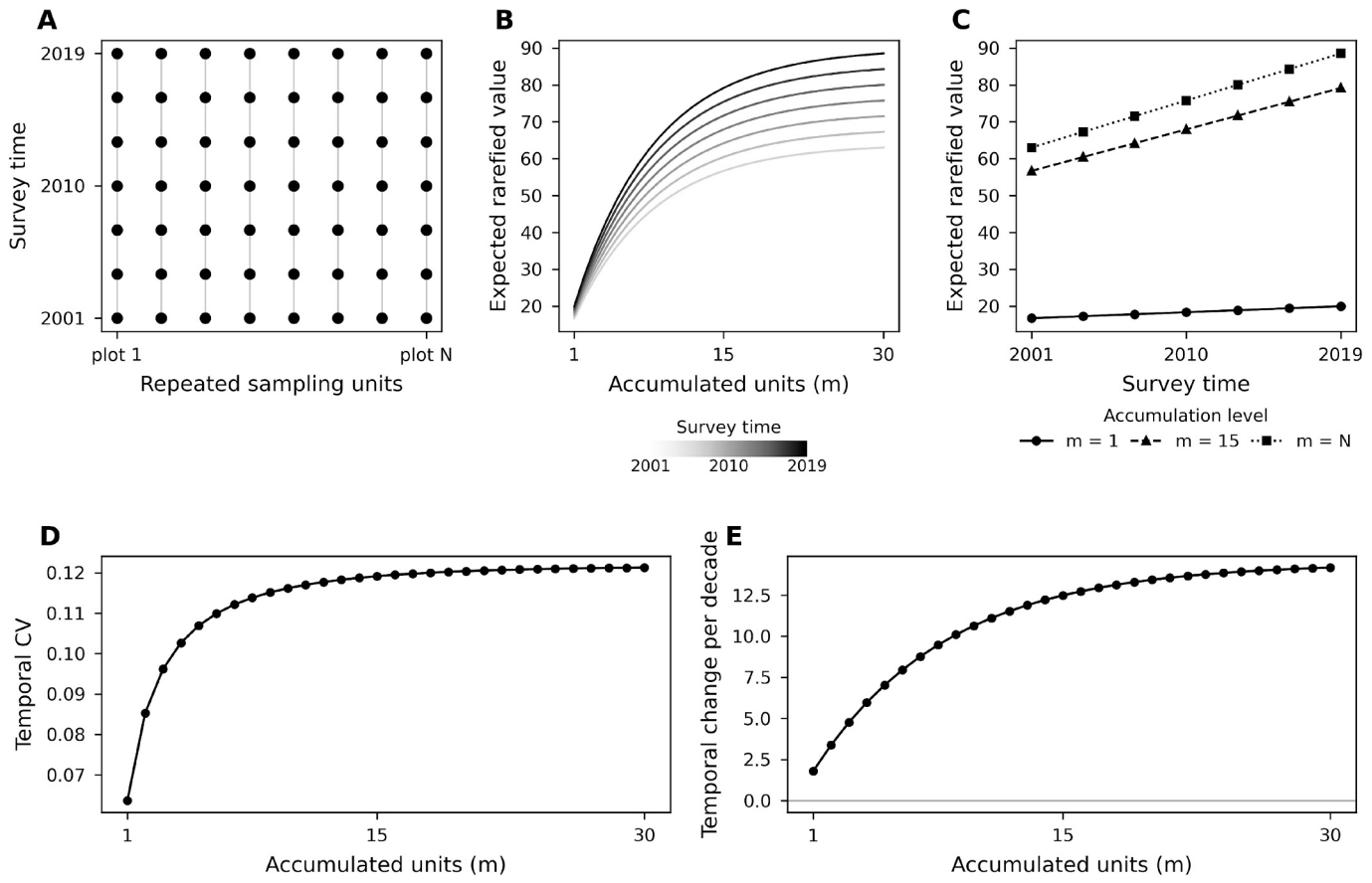


Fig. 1. Workflow of temporal rarefaction profiles for repeated ecological surveys. (A) Comparable sampling units are revisited across survey occasions. (B) A sample-based rarefaction curve is calculated independently for each survey occasion, using the cumulative number of sampling units, *m*, as the rarefaction axis; line shading and the legend indicate survey time. (C) At any fixed value of *m*, the corresponding expected rarefied values define a temporal trajectory across survey occasions; selected trajectories for $m = 1$, an intermediate value of *m*, and $m = N$ are shown. (D) Temporal variability is calculated across survey occasions at each *m* to obtain the temporal variability profile. (E) Directional temporal change is estimated at each *m* and expressed as temporal change per decade.

functional structure of the assemblage changes from individual plots to the full sampled community (Rao, 1982; Ricotta et al., 2012). The framework can also be applied to community descriptors that are not diversity measures but remain ecologically interpretable along the same accumulation gradient. In this study, the Euclidean distance between the community-weighted mean trait vector of a rarefied subset and a treatment-specific baseline was used to quantify the magnitude of functional displacement from a reference state. This metric does not describe the spread or volume of trait space; it describes movement in dominant trait composition relative to a reference state. Calculating it along the rarefaction curve makes it possible to evaluate whether directional functional change is already visible at the alpha scale or becomes clearer only after plots are pooled towards sampled gamma diversity.

Rarefaction profiles across repeated surveys are then obtained in the same way for all selected metrics. A rarefaction curve is calculated independently for each survey year, and the temporal variability among annual curves is evaluated at each number of accumulated sampling units. The interpretation of the resulting profile depends on the metric: for richness and Shannon diversity it describes temporal variability in taxonomic diversity; for functional richness, Rao's *Q* or *FDis* it describes temporal variability in functional diversity; for *CWM* displacement it describes temporal variability in directional functional reorganisation.

Unlike species–time or species–time–area relationships, temporal rarefaction profiles do not treat time as the dimension along which species are accumulated (Adler et al., 2005; Adler and Lauenroth, 2003; Preston, 1960; White et al., 2006). Each survey year is instead represented by its own sample-based rarefaction curve, calculated along the same gradient of accumulated sampling units. Temporal change is then evaluated by comparing these annual curves at each value of *m*, so that both variability and directionality can be measured at equivalent positions between the alpha and sampled-gamma scales. Equivalently, for any fixed value of *m*, the expected rarefied values can be viewed as a temporal trajectory across survey occasions, from which temporal variability and temporal change are subsequently calculated (Fig. 1).

The temporal variability profile for metric *D* can therefore be expressed as:

$$TV_D(m) = Var_t\left[R_{D,t}(m)\right] \tag{2}$$

For comparisons among metrics with different units or magnitudes, a scale-standardised version can be used:

$$CVTV_D(m) = \frac{SD_t\left[R_{D,t}(m)\right]}{\overline{R_D(m)}} \tag{3}$$

where $\overline{R}_D(m)$ is the mean expected rarefied value across survey times at accumulation level *m*.

The coefficient of temporal variation is calculated after the annual rarefaction curves have been obtained. For a given value of *m*, it takes the expected rarefied value from each survey year and measures how variable those annual values are through time. It therefore summarises temporal variability at a fixed level of sampling-unit accumulation: for example, variability among years in expected alpha diversity when $m = 1$, and variability among years in expected sampled gamma diversity when $m = N$. The original rarefaction curves remain necessary

because they show the annual accumulation patterns from which the temporal variability profile is derived. A high value of *CVTVD(m)* means that years differ strongly relative to their temporal mean when diversity is calculated from m sampling units. A low value means that years are similar at that same level of aggregation. *CV* is useful in this context because it standardises temporal dispersion by the temporal mean, which itself can change substantially along an accumulation curve. However, *CV* can become unstable when the mean approaches zero, may be sensitive to extreme observations and skewed temporal distributions, and does not distinguish whether temporal variability arises from directional trends, episodic disturbances, cyclic dynamics or irregular fluctuations. Absolute *SD* and alternative information-based measures therefore provide useful complementary descriptions of temporal variability (Chao et al., 2025).

A complementary temporal trend profile can be calculated by modelling the expected rarefied value at each level of accumulation as a function of time. For each metric D and each value of m, the annual rarefied values can be described as:

$$R_{D,t}(m) = \alpha_D(m) + \beta_D(m)\tau_t + \varepsilon_{D,t}(m) \quad (4)$$

where τ_t is the numerical representation of survey time, $\alpha_D(m)$ is the fitted intercept at accumulation level m, $\beta_D(m)$ is the temporal slope of the rarefied metric at that same accumulation level and $\varepsilon_{D,t}(m)$ is the residual deviation of the observed survey-specific rarefied value from the fitted temporal trend for metric D, survey time t and accumulation level m. The sequence of $\beta_D(m)$ values along $m = 1, 2, \ldots, N$ defines the temporal trend profile. Negative slopes indicate decreasing rarefied diversity or displacement through time, positive slopes indicate increasing values, and slopes close to zero indicate weak directional change at the corresponding level of accumulation. In the worked example, τ_t was expressed in calendar years, so $\beta_D(m)$ represents change per year. For reporting and graphical presentation, this annual coefficient was multiplied by 10 and expressed as temporal change per decade. This trend profile is not intended to replace formal time-series modelling when temporal autocorrelation, non-linearity or change-points are the primary focus. Its purpose is to make the direction of temporal change explicit along the same sample-based accumulation gradient used for the variability profile.

The temporal variability and trend profiles can be read as a scale-explicit link between alpha and sampled gamma diversity. At $m = 1$, diversity is calculated for one sampling unit, so the profile describes variability or directional change in expected alpha diversity among survey years. At $m = N$, all sampling units are pooled, so the profile describes variability or directional change in sampled gamma diversity within the sampled focus. Alpha and sampled gamma are therefore defined by the sampling design: the grain is the individual sampling unit, and the focus is the full set of units included in the analysis (Scheiner et al., 2011; Tuomisto, 2010a, 2010b; Whittaker, 1960).

The values between $m = 1$ and $m = N$ show how temporal variability and temporal trend change as additional sampling units are added. These intermediate positions are beta-relevant because among-unit heterogeneity affects the transition from expected alpha diversity to sampled gamma diversity, but they do not directly measure spatial scale, beta-diversity processes, temporal synchrony or compensation; these mechanisms require additional compositional, temporal or spatial analyses.

Rarefaction profiles for repeated surveys belong to the same broad rarefaction family as spatially constrained and spatially explicit rarefaction, but they use the rarefaction curve for a different purpose. Spatially constrained rarefaction modifies the accumulation process itself by accounting for the spatial arrangement of sampling units, because nearby units may contain similar communities and should not always be treated as freely exchangeable (Bacaro et al., 2016; Chiarucci et al., 2009). Temporally repeated sample-based rarefaction does not impose either a temporal ordering or a spatial constraint on the sampling units within a curve. Instead, a separate sample-based rarefaction curve is calculated for each survey year, and the set of annual curves is then compared along the same alpha–sampled-gamma accumulation gradient. The connection with spatial rarefaction is therefore methodological rather than identical in design: both approaches use the full rarefaction curve to retain information that would be lost in a single endpoint, but spatial rarefaction focuses on the spatial arrangement of sampling units, whereas the repeated-survey framework focuses on the temporal variability and directionality among independently calculated rarefaction curves. If permanent plots are spatially structured, the two approaches could be combined by calculating temporal rarefaction profiles from spatially constrained subsets, but this is an extension rather than a requirement of the framework.

The shape of the temporal variability profile provides a diagnostic description of how temporal differences change with sampling-unit accumulation. Four idealised diagnostic patterns are illustrated schematically in Fig. 2. Low temporal variability at both $m = 1$ and $m = N$ indicates that expected plot-level alpha diversity and sampled gamma diversity remain relatively stable across survey occasions, although substantial changes may still occur within individual sampling units.

Low variability at $m = 1$ combined with higher variability near $m = N$ indicates that temporal differences become more evident as sampling units are pooled. Depending on the ecological and spatial context, possible explanations include changes involving low-occupancy or spatially restricted species, local colonisation or extinction events, or increasing differentiation among sampling units. These explanations are non-exclusive and cannot be identified from the profile alone. High variability at $m = 1$ followed by lower variability near $m = N$ indicates that temporal differences are progressively attenuated during aggregation. This pattern may be compatible with asynchronous or compensatory dynamics among sampling units, but demonstrating these mechanisms requires an explicit analysis of temporal synchrony or compositional change. High variability across the full curve indicates that temporal differences remain evident from individual sampling units to the full sampled community. When temporal trend profiles are considered together with variability profiles, the framework also distinguishes whether these differences are mainly non-directional, directional, or both. These patterns are intended as an interpretative guide for empirical profiles, not as a formal classification algorithm, and process-based interpretations should be supported by independent ecological, compositional or spatial evidence. Fig. 2 is therefore presented on relative, non-numerical axes and should be interpreted in terms of profile shape rather than absolute values.

The temporal variability profile can also be summarised by a single value, although this summary should not replace the interpretation of the curve. In this study, we summarised the temporal variability profile using the discrete sum of temporal CV values across accumulation levels (hereafter referred to as *AUC*):

$$AUC_{CVTV,D} = \sum_{m=1}^{N} CVTV_D(m) \quad (5)$$

This value measures the overall amount of temporal variability expressed along the rarefaction curve. It is useful for comparing treatments or groups when the same number of sampling units is available. If datasets have different numbers of sampling units, the *AUC* should be calculated over a common range of m or normalised by the number of accumulation levels included in the calculation. Because similar *AUC* values can arise from differently shaped profiles, *AUC* is retained as a supporting summary and should be interpreted together with the endpoints and the full curve. The temporal trend profile can be summarised analogously, but its full shape remains the primary result.

Rarefaction profiles for repeated surveys are intended to describe the accumulation level at which temporal variability and directional change are expressed. They do not, by themselves, identify the species responsible for compositional change, or partition turnover into replacement and nestedness components. Temporal beta-diversity analyses remain

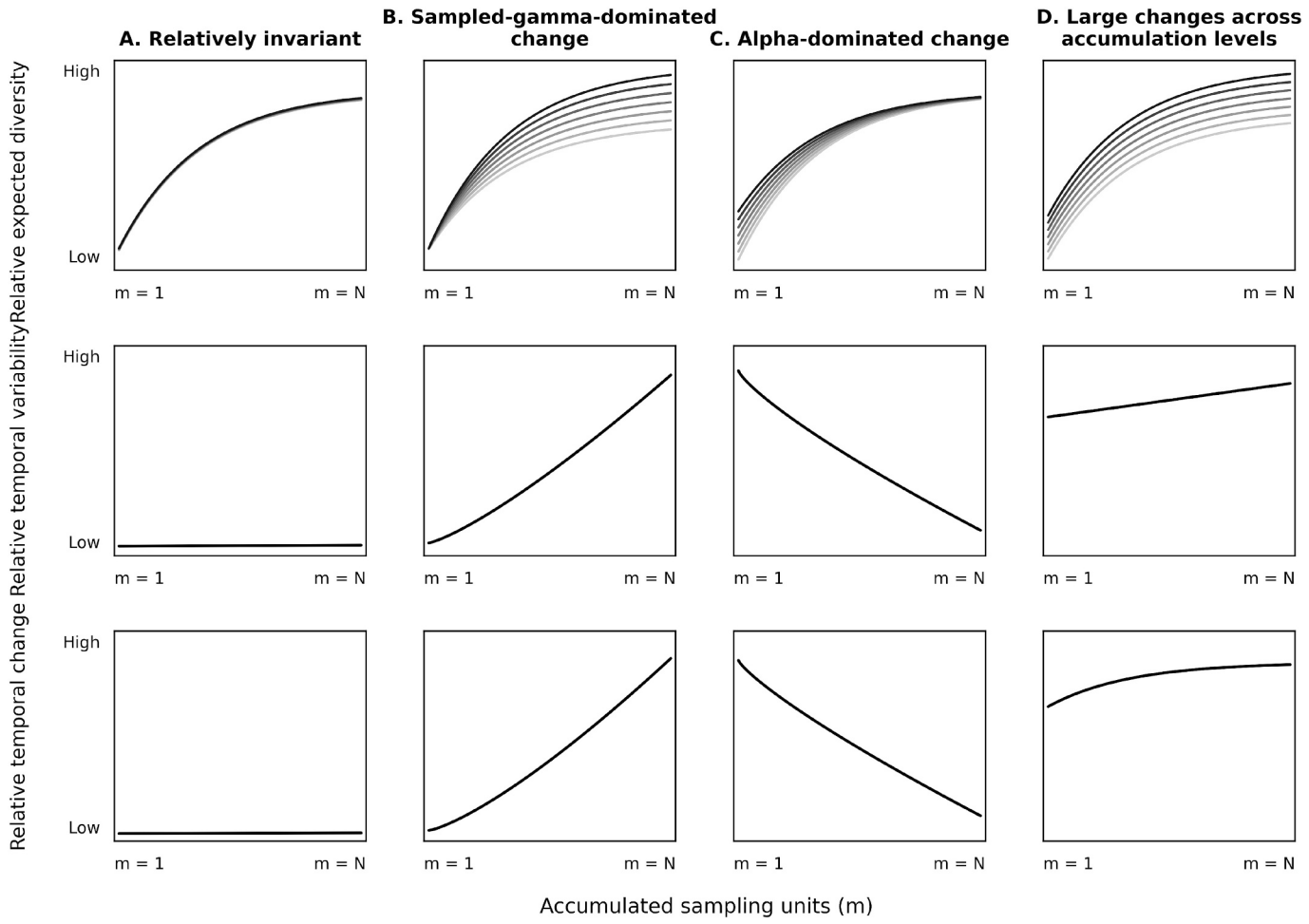


Fig. 2. Conceptual diagnostic patterns for rarefaction profiles across repeated surveys. The figure is schematic and does not represent results from a quantitative simulation. The first row shows idealised rarefaction curves across repeated survey occasions. The second row shows the corresponding relative temporal-variability profiles, and the third row shows the corresponding directional temporal-change profiles. Axes are intentionally shown without numerical values because the diagnostic interpretation concerns profile shape and relative change along the accumulation gradient from $m = 1$ to $m = N$, rather than particular numerical magnitudes. The four diagnostic types represent (A) relatively invariant profiles, (B) sampled-gamma-dominated change, (C) alpha-dominated change, and (D) large changes across accumulation levels.

necessary when the objective is to quantify changes in species composition, identity replacement or nestedness through time (Hillebrand et al., 2018; Magurran et al., 2019; Shimadzu et al., 2015). Trend profiles make direction explicit along the accumulation curve, but they should not be interpreted as a substitute for full time-series models when temporal autocorrelation, non-linearity, disturbance timing or change-points are the primary questions. Temporal rarefaction profiles provide a complementary summary by showing whether temporal variability and directional change are mainly associated with alpha diversity, sampled gamma diversity or the transition between the two as sampling units are accumulated. This makes the approach useful for monitoring designs in which sampling units are replicated in space and revisited through time, especially when a single annual diversity value would obscure whether the temporal signal is local, cumulative, directional or maintained across the alpha–sampled-gamma gradient.

3. Worked example and analytical implementation

We used the Monte Labbro long-term grassland experiment as a worked example to illustrate the repeated-survey rarefaction framework. The dataset is used to demonstrate the analytical workflow and to evaluate associations between grazing status and the resulting profiles; it is not treated as a direct test of rare-species contributions, temporal synchrony, spatial compensation or temporal beta-diversity mechanisms. The site is a semi-natural calcareous grassland in southern Tuscany, Italy, previously used to analyse how grazing and climatic extremes affect taxonomic and functional community structure over a long experimental period (Pavanetto et al., 2025). The experiment is located near the summit of Monte Labbro (42°49′13″ N, 11°31′33″ E), within a predominantly calcareous massif. The broader restoration area covers approximately 17 ha and ranges from 1089 to 1193 m a.s.l.; previous site descriptions report mean annual rainfall of approximately 1002–1469 mm and mean annual temperatures of 12.1–12.5 °C (Maccherini et al., 2007, 2009). The area was grazed for centuries, predominantly by sheep, but declining grazing pressure after the 1960s promoted secondary succession and shrub encroachment. The experimental plots were established in an overgrown pasture restored by shrub cutting around 2000–2001, where *Prunus spinosa* was the dominant shrub before restoration. Grazing was subsequently maintained primarily by donkeys, at approximately 0.5 animals ha − 1 year−1, with occasional grazing by sheep and cattle (Pavanetto et al., 2025).

In 2001, sixteen 3 × 5-m experimental plots were established in four randomised blocks, with four plots per block. Vegetation was recorded in a permanent 1 × 2-m subplot centred within each experimental plot; thus, the observational grain represented by $m = 1$ in the present analysis is 2 m^2. The dataset comprises 16 permanent plots arranged in

four experimental blocks and surveyed on 16 occasions between 2001 and 2019. Surveys were conducted in 2001–2004, 2006–2016 and 2019; the time series is therefore based on repeated permanent-plot surveys but is not an uninterrupted annual sequence. For the present methodological application, plots were grouped according to grazing status, producing two balanced groups of eight grazed and eight ungrazed plots for each survey occasion. The original sowing factor was not retained in the present grouping. Block was likewise not used as an explanatory factor in the repeated-survey rarefaction analysis; however, the original four-block structure was retained when defining spatial resampling units for the primary sampling-uncertainty analysis. Accordingly, each treatment-specific rarefaction curve accumulates eight permanent 2-m^2 vegetation subplots. The endpoint at $m = N = 8$ represents the cumulative diversity of these eight sampling units within the defined treatment sampling focus; it should not be interpreted as the diversity of the entire c. 17-ha restoration area or as the diversity of a single contiguous 16-m^2 area. Final plot counts by treatment and survey occasion are provided in the CSV outputs listed in Supplementary Table S1.

The community data were organised as a sampling-unit-by-species matrix including 131 vascular plant taxa, with percentage cover used as the abundance measure. Taxonomic rarefaction was calculated from the full community matrix using the permanent 1 × 2-m vegetation subplots as the sampling units. For species richness, we used the classical sample-based formulation of rarefaction, in which the expected number of accumulated species is evaluated for $m = 1, 2, \ldots, N$ plots drawn without replacement from the full set of N plots. Expected richness was obtained from the incidence structure of species among plots using the analytical solution originally derived by Shinozaki and later rediscovered in the rarefaction literature (Chiarucci et al., 2008; Colwell et al., 2004; Shinozaki, 1963). For abundance-weighted taxonomic metrics, including Shannon and Simpson diversity, percentage covers were pooled within each combination of m plots and the diversity metric was calculated on the resulting pooled assemblage.

Functional analyses were based on the trait-covered dominant species subset described by Pavanetto et al. (2025). For each value of m, the selected plots were pooled, and species relative covers and the trait-distance structure were used to calculate the functional metrics. Further metric-specific details are provided in the Functional extension subsection.

The functional trait matrix included vegetative leaf area, specific leaf area, leaf dry matter content, turgor loss point, leaf nitrogen concentration, leaf carbon concentration and carbon isotope composition. These traits capture major axes of plant ecological strategy, including leaf economics and resource acquisition (Reich, 2014; Wright et al., 2004), drought-related hydraulic tolerance (Bartlett et al., 2012) and leaf chemical differentiation associated with resource use (Díaz et al., 2016). After nomenclatural harmonisation, 31 species with complete or imputed trait information matched the community matrix. Functional rarefaction profiles are therefore interpreted as profiles of dominant-species functional structure, rather than as a complete representation of the functional diversity of the entire species pool.

3.1. Repeated-survey rarefaction analysis

For each treatment group and survey year, we calculated a sample-based rarefaction curve using plots as sampling units. Each curve represents the expected value of a diversity metric as a function of the cumulative number of plots m, with m ranging from one plot to the total number of plots available in that treatment-year. For each value of m, combinations of m plots were drawn without replacement from the full set of N plots. Species percentage covers were pooled across the selected plots, and the target metric was calculated on the resulting pooled assemblage. The procedure therefore follows the classical sample-based rarefaction approach, in which diversity is evaluated against increasing sampling effort expressed as the number of accumulated sampling units, rather than as the number of accumulated individuals (Colwell et al., 2004; Gotelli and Colwell, 2001).

In the Monte Labbro dataset, each treatment-year contained eight plots, allowing all possible combinations of m plots to be evaluated for each point of the rarefaction curve. For larger datasets, the same expected values can be estimated by repeated random resampling of plot combinations without replacement. For each treatment-year and each value of m, the mean value across combinations was retained as the expected rarefied diversity, and the 2.5% and 97.5% quantiles were retained as rarefaction intervals. These intervals describe within-year variability among possible combinations of plots and are therefore distinct from the temporal variability profile calculated across survey years (Fig. S1). Species richness and Shannon diversity were used as the main taxonomic metrics, while Simpson diversity was retained as a supporting metric.

Temporal variability profiles were then derived from the set of annual rarefaction curves. For each metric and each value of m, we calculated the variance, standard deviation and coefficient of variation of the expected rarefied values across survey years. The resulting profile describes how temporal variability changes along the rarefaction curve, from single plots to the full sampled community. The value at $m = 1$ was interpreted as temporal variability in expected alpha diversity, because diversity is evaluated at the grain of one plot. The value at $m = N$ was interpreted as temporal variability in sampled gamma diversity, because all plots in the treatment-year are pooled. Values between these limits describe the alpha–sampled-gamma accumulation profile, showing whether temporal variability is concentrated at the plot scale, emerges only after plots are pooled, or is maintained across the full accumulation gradient. The area under the temporal coefficient-of-variation profile was used as a whole-profile numerical summary, but the shape of the profile remained the primary ecological output.

To assess whether the empirical conclusions depended on the use of *CV* as the temporal variability descriptor, we performed a sensitivity analysis using two complementary alternatives. First, temporal *SD* was used as a non-standardised measure of absolute temporal dispersion. Second, we applied the information-based temporal stability framework of Chao et al. (2025) using the *iSTAY R* package (version 1.1.0). Information-based stability was calculated at $q = 1$ and $q = 2$ for the vector of annual expected rarefied values at each *treatment* × *metric* × m combination and converted to information-based variability as 1 − stability, so that larger values indicate greater temporal variability. Information-based variability at $q = 1$ was used as the principal information-based alternative, whereas $q = 2$ provides a measure mathematically related to conventional *CV*-based stability. As an additional robustness audit, information-based variability was also evaluated over the continuum $q = 0.1$–2.0. All main metric profiles were based on the same 16 survey dates at each value of m. Sensitivity results are reported in the Supplementary Material (Fig. S2; Tables S9–S10).

Temporal trend profiles were calculated from the same survey-specific rarefaction curves. For each metric, treatment group and value of m, we fitted a linear model relating the expected rarefied value to the actual calendar year of each survey. The fitted coefficient therefore represents temporal change per year. For reporting and graphical presentation, the coefficient was multiplied by 10 and expressed as temporal change per decade. The fitted slope was retained as the temporal trend estimate at that position of the accumulation curve.

The resulting sequence of slopes along ($m = 1, 2, \ldots, N$) describes whether directional change is concentrated at the alpha-diversity scale, becomes stronger towards the sampled-gamma scale, or remains similar along the accumulation profile. For each metric and treatment, we reported slopes at $m = 1$ and $m = N$ as alpha-scale and sampled-gamma-scale summaries, respectively. These trend profiles were used as descriptive summaries of directional change along the rarefaction gradient, not as full time-series models of temporal autocorrelation, non-linearity or change-points.

3.2. Functional extension

Functional temporal rarefaction used the same sample-based accumulation scheme as the taxonomic analysis, but the accumulated quantity was a functional descriptor rather than species richness or taxonomic diversity. Species were represented in a standardised trait space, and functional metrics were calculated on the pooled assemblage obtained for each combination of m plots. Rao's quadratic entropy was used as an abundance-weighted measure of pairwise functional dissimilarity among species (Rao, 1982), functional dispersion was used to describe the abundance-weighted dispersion of species around the community centroid (Laliberté and Legendre, 2010), and functional richness was estimated as the convex-hull area occupied in the first two axes of the standardised trait ordination (Villéger et al., 2008). These metrics were retained because they summarise complementary properties of dominant-species functional structure: average trait dissimilarity, dispersion around a centroid and extent of occupied trait space. For each functional metric, we derived both temporal variability profiles and temporal trend profiles along the same accumulation gradient used for the taxonomic analysis. Functional profiles were therefore interpreted by asking whether temporal variation or directional change in trait structure was already visible at the alpha-diversity scale, became clearer towards the sampled-gamma scale, or remained similar as plots were progressively pooled.

We also calculated the Euclidean distance between the community-weighted mean trait vector of each rarefied assemblage and the treatment-specific baseline in the first survey year. This quantity is not a functional diversity metric, because it does not measure dispersion, dissimilarity or trait-space occupancy. It was included as a directional descriptor of functional reorganisation, allowing us to evaluate whether the dominant trait composition moved away from the initial state as plots were accumulated. Functional richness and *CWM* displacement are emphasised because they represent two distinct ecological signals: the amount of occupied dominant-species trait space and the direction of trait-composition change relative to the baseline. For *CWM* displacement, positive temporal slopes indicate increasing departure from the first-year treatment-specific baseline, whereas slopes close to zero indicate little systematic temporal change in the magnitude of displacement at the corresponding accumulation level. Rao's *Q* and functional dispersion are reported as supporting functional metrics in the Supplementary Material.

Sensitivity analyses confirmed that the principal treatment contrasts were robust to the choice of temporal variability measure (Fig. S2; Tables S9–S10). For species richness, Shannon diversity, functional richness and *CWM* displacement, the sign of the Ungrazed − Grazed contrast was unchanged at all eight accumulation levels when temporal *SD* or information-based variability at $q = 1$ or $q = 2$ was used instead of *CV*. Information-based variability at $q = 1$ closely reproduced the shape of the *CV* profiles, with within-treatment Spearman correlations ranging from 0.952 to 1.000 for the four main metrics; correlations between the corresponding treatment-contrast profiles ranged from 0.857 to 1.000. The $q = 2$ profiles were perfectly rank-correlated with *CV* within treatments, as expected from their mathematical relationship. Temporal *SD* provided a complementary pattern. Although it retained the direction of all principal treatment contrasts at every accumulation level, its profile shape did not always coincide with that of *CV*. For species richness, temporal *SD* increased with *m* whereas temporal *CV* decreased in both treatments. Absolute among-year dispersion in accumulated richness therefore increased as plots were pooled, while variability relative to the increasing temporal mean declined. Across the information-based continuum $q = 0.1$–2.0, the sign of the treatment contrast was retained at every *m* for all four main metrics.

3.3. Sampling uncertainty and sensitivity to the spatial resampling unit

The 2.5%–97.5% intervals associated with each annual rarefaction curve quantify variation among possible combinations of plots within a survey occasion and should not be interpreted as sampling uncertainty around the temporal profiles derived across surveys. We therefore quantified sampling uncertainty separately using a combined spatial and temporal non-parametric bootstrap with 9999 replicates.

For the primary spatial bootstrap, the four experimental blocks were sampled with replacement. Each selected block retained its four permanent plots, including two grazed and two ungrazed plots, together with their complete temporal trajectories. Block was used only as the spatial resampling cluster and was not included as an explanatory factor. This procedure preserves the original experimental layout and the repeated-measures structure while maintaining Grazed versus Ungrazed as the only biological grouping used in the temporal rarefaction analysis.

To incorporate uncertainty associated with the finite number of survey occasions, the 16 observed surveys were also sampled with replacement. The same temporal draw was applied to grazed and ungrazed plots, and the original calendar years associated with the selected observations were retained when estimating temporal change. For each combined bootstrap replicate, the annual rarefaction profiles and their derived temporal *CV* and temporal-change profiles were recalculated. Bootstrap variance, standard errors and percentile 95% uncertainty intervals were then obtained for temporal *CV* and temporal change at each value of *m*, whole-profile *AUC* summaries, Ungrazed − Grazed contrasts, and differences between accumulation levels. The contrast $CV(m = N) - CV(m = 1)$ was retained as the principal endpoint comparison, while all pairwise differences among values of *m* were calculated as supplementary numerical outputs. For *CWM* displacement, the first-year treatment-specific baseline *CWM* was re-estimated within each spatial bootstrap configuration.

As a sensitivity analysis, we repeated the complete procedure without using the experimental blocks as spatial resampling clusters. Instead, the eight permanent-plot trajectories were sampled with replacement independently within the Grazed and Ungrazed groups, while the temporal resampling procedure remained unchanged. This alternative analysis treats permanent plots within each grazing group as the spatial resampling units and was used to assess whether the uncertainty estimates depended materially on retention of the original block structure.

3.4. Null expectations

Sampling uncertainty and ecological null expectations address different questions. The bootstrap analysis described above evaluates uncertainty associated with the finite set of spatial and temporal observations. We additionally used two null models to ask whether selected observed profiles differed from explicitly defined ecological reference processes.

First, we evaluated the richness profiles against a random species-allocation expectation. For each grazing group and survey occasion, the observed presence–absence matrix was randomised using the binary *r1* null model implemented in *vegan*. This procedure preserves the observed richness of each plot exactly and uses the observed marginal frequencies of species as selection probabilities, while otherwise randomising species identities among plots. We generated 4999 null assemblages independently for each treatment-year. For each randomised assemblage, expected richness after accumulating m plots was calculated analytically from the species incidence frequencies, f_s, as

$$E[S_m] = \sum_s \left[1 - \frac{\binom{N - f_s}{m}}{\binom{N}{m}} \right].$$

Temporal *CV* and temporal change per decade were then recalculated across the 16 survey occasions for every null replicate. Observed values were compared with pointwise 95% null envelopes. We also used

a global maximum-deviation statistic based on the largest absolute standardised departure from the null expectation across m. Because the *r1* model preserves plot richness exactly, observed and null values are identical at $m = 1$; global tests for this null therefore used $m = 2, \ldots, N$. We additionally evaluated the endpoint difference $CV(m = N) - CV(m = 1)$.

Second, we evaluated the taxonomic Grazed–Ungrazed contrasts against an exact treatment-label null distribution matched to the blocked experimental design. Within each of the four blocks, two of the four permanent plots were assigned the Grazed label and two the Ungrazed label, and each assignment was held constant over the complete temporal trajectory of the permanent plot. All (6^4 = 1296) admissible assignments were enumerated. Richness and Shannon rarefaction profiles were recalculated for every assignment, followed by temporal *CV*, temporal change per decade and the corresponding Ungrazed − Grazed contrasts at every *m*. Pointwise 95% null envelopes, global maximum-deviation tests and whole-profile *AUC* contrasts were calculated from these exact randomisation distributions. This null model tests whether the observed taxonomic grazing contrasts exceed those expected if grazing labels were unrelated to permanent-plot trajectories while retaining the original blocked and balanced experimental structure.

Formal grazing-label null tests were not implemented for functional metrics in the present analysis because each label reassignment would require recalculating the treatment-specific functional objects and, for *CWM* displacement, the corresponding first-year baseline vectors. Functional treatment differences are consequently interpreted descriptively and evaluated through the sampling-uncertainty and sensitivity analyses described above.

3.5. Trait coverage and robustness checks

Because functional analyses were based on the dominant species with available trait information, trait coverage was quantified for each plot-year as the proportion of total vegetation cover represented by trait-matched species. Functional metrics were calculated only for pooled subsets in which trait-matched species accounted for at least 50% of the pooled cover. Subsets below this threshold were excluded, and expected rarefied values were calculated from the remaining valid subsets. Robustness was assessed by repeating the functional rarefaction analyses using stricter pooled trait-cover thresholds of 60% and 70%. We also repeated the analyses after excluding plot-years in which trait-matched species represented less than 50% of total cover. These checks were used to assess whether the functional profiles were robust to variation in trait coverage, rather than being driven by a small number of low-coverage plot-years. Robustness checks were evaluated for the main functional contrasts retained in the paper, with particular attention to functional richness and *CWM* displacement, because these metrics represented the two primary functional responses discussed in the Results. Trait-coverage diagnostics and sensitivity results are reported in the Supplementary Material.

All analyses were conducted in *R* (R Core Team, 2026). The workflow was organised into separate steps for data preparation, repeated-survey rarefaction analysis, temporal trend estimation, and final figure and table production. Data manipulation used *dplyr* and *tidyr*, graphical outputs were produced with *ggplot2* (Wickham, 2016), and resampling procedures used reproducible base *R* routines. Information-based temporal variability for the sensitivity analyses was calculated using the *iSTAY* package (version 1.1.0). The analytical workflow was implemented as a reproducible stand-alone script and associated *temporal_rarefy()* development function, available through the project repository. The function returns survey-specific rarefaction curves, within-year rarefaction intervals, temporal variability profiles, temporal trend profiles, alpha- and sampled-gamma-scale summaries, whole-profile summaries and group contrasts. *Rarefy* already provides sample-based rarefaction tools for taxonomic, functional, phylogenetic and user-defined diversity metrics, including spatially explicit rarefaction (Thouverai et al., 2026). The repeated-survey rarefaction workflow extends this logic to repeated ecological surveys and is intended as a future integration into the *Rarefy* framework rather than as a manuscript-specific analysis only.

4. Results

4.1. Taxonomic rarefaction profiles across repeated surveys

Taxonomic rarefaction profiles across repeated surveys showed clearer temporal variation in ungrazed than in grazed communities (Fig. 3). In grazed plots, annual rarefaction curves for species richness and Shannon diversity remained closely grouped from the alpha-diversity scale, $m = 1$, to the sampled-gamma-diversity scale $m = 8$. In ungrazed plots, annual curves were more widely separated, particularly in the first part of the rarefaction curve, where expected diversity is calculated from one or few plots. The temporal *CV* profiles confirmed that this larger among-year variation was strongest near the alpha-diversity scale and declined as plots were progressively accumulated (Fig. 4).

For species richness, the area under the temporal *CV* profile was 0.863 in grazed plots and 1.598 in ungrazed plots (Table 1). At the alpha-diversity scale, temporal *CV* was 0.153 in grazed plots and 0.268 in ungrazed plots. At the sampled-gamma-diversity scale, temporal *CV* was 0.088 in grazed plots and 0.164 in ungrazed plots. Shannon diversity showed the same treatment contrast, with *AUC* values of 0.441 in grazed plots and 1.090 in ungrazed plots. Thus, both main taxonomic metrics showed higher temporal variability in ungrazed plots. Temporal variability decreased along the alpha–sampled-gamma accumulation profile for species richness in both treatments and for Shannon diversity in ungrazed plots, whereas Shannon diversity remained nearly constant in grazed plots (Fig. 4; Table 1).

Temporal trend profiles showed that taxonomic differences were not limited to variability, but also involved the direction of change through time. Species richness declined more strongly in ungrazed plots than in grazed plots along the full accumulation gradient. At $m = 1$, temporal change was −9.90 species per decade in ungrazed plots and − 2.64 species per decade in grazed plots. At $m = N$, the contrast was even clearer, with temporal change of −14.03 species per decade in ungrazed plots and − 0.33 species per decade in grazed plots. Shannon diversity showed a similar directional signal, with stronger negative temporal change in ungrazed plots and much weaker change in grazed plots. In ungrazed plots, Shannon diversity declined by 0.625 units per decade at $m = 1$ and by 0.350 units per decade at $m = N$.

The annual values at the alpha and sampled-gamma scales are provided in Supplementary Table S1, allowing the survey-year values underlying these profiles to be inspected directly. The alpha–sampled-gamma trajectories are shown in Fig. S3. These results show that the larger temporal *CV* in ungrazed plots was associated with broader among-year variation in both expected alpha diversity and sampled gamma diversity, whereas grazed plots retained a narrower taxonomic range across the survey period. The trend profiles further indicated that grazing exclusion was associated not only with higher taxonomic variability, but also with a stronger directional decline in taxonomic diversity.

4.2. Functional rarefaction profiles across repeated surveys

Functional rarefaction profiles across repeated surveys did not reproduce the taxonomic pattern (Fig. 5). Functional richness, calculated as the convex-hull area occupied in the first two axes of the standardised trait ordination, was more temporally variable in grazed plots. In contrast, the distance from the baseline community-weighted mean trait vector was more temporally variable in ungrazed plots. The *AUC* of the temporal *CV* profile for functional richness was 0.700 in

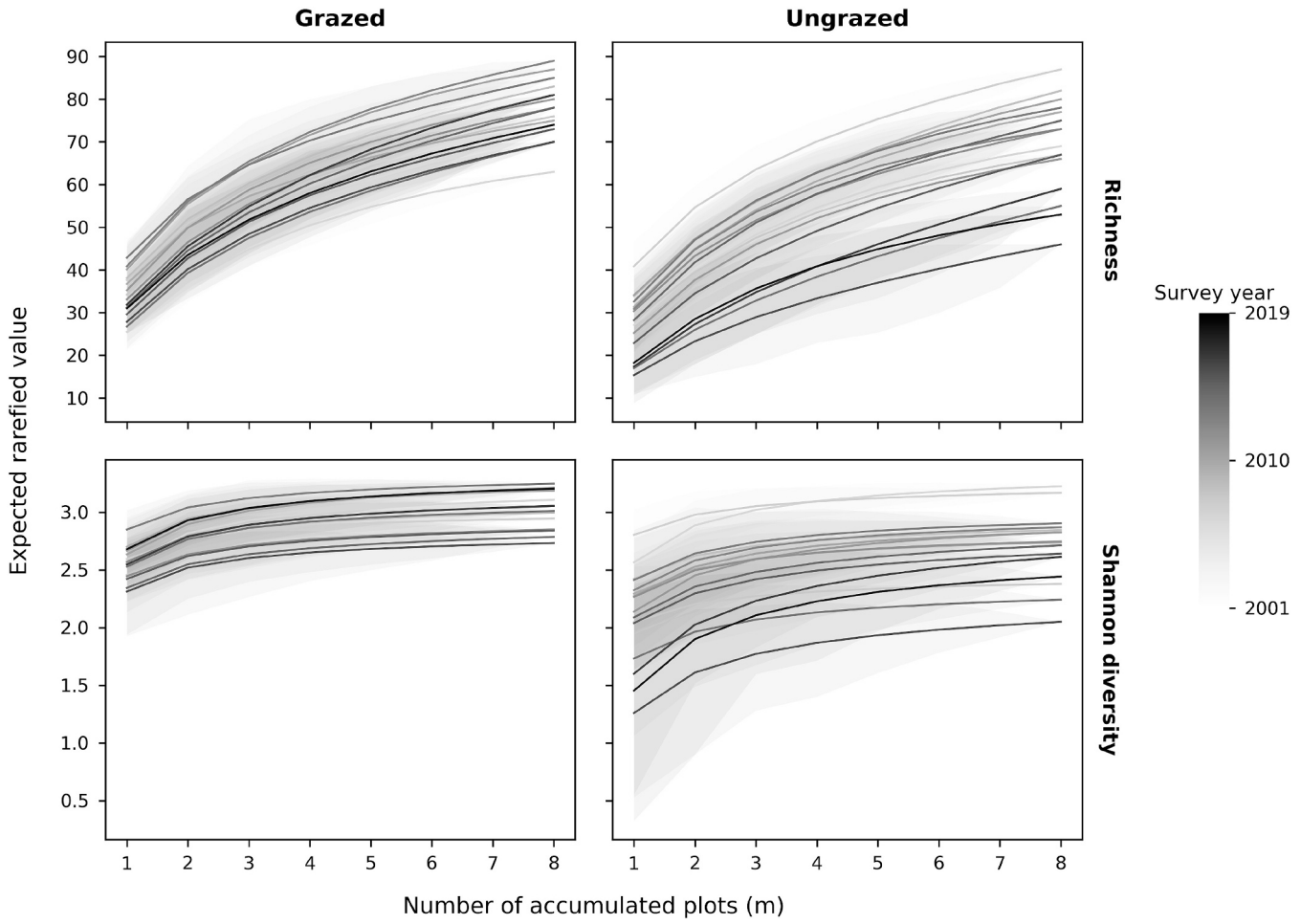


Fig. 3. Taxonomic rarefaction profiles across repeated surveys for the Monte Labbro worked example. Curves were calculated independently for each survey year and grazing group. Lines represent survey-specific expected rarefied values; grey scale indicates survey year. Ribbons represent the 2.5% and 97.5% quantiles across plot combinations for each annual curve, and therefore describe within-year variation among possible combinations of plots.

grazed plots and 0.377 in ungrazed plots (Table 1). The corresponding *AUC* values for *CWM* displacement were 2.972 in grazed plots and 4.135 in ungrazed plots.

These two functional profiles described different aspects of temporal functional change. Functional richness measured how the amount of occupied dominant-species trait space varied through time along the alpha–sampled-gamma accumulation profile. *CWM* displacement measured how strongly the dominant trait composition moved away from the first-year, treatment-specific baseline as plots were accumulated. The contrast between these two metrics shows that temporal variation in functional trait-space occupancy and temporal variation in directional trait-composition change were not equivalent.

Functional trend profiles reinforced this distinction. The temporal trend in functional richness became more positive with increasing m in grazed plots, whereas ungrazed plots showed negative trends at both endpoints and values close to zero at intermediate accumulation levels. At $m = N$, temporal change in functional richness was +0.669 per decade in grazed plots and − 0.226 per decade in ungrazed plots. *CWM* displacement showed the opposite ecological signal: departure from the first-year trait-composition baseline increased more strongly in ungrazed plots than in grazed plots. At $m = N$, temporal change in *CWM* displacement was +0.659 per decade in ungrazed plots and + 0.153 per decade in grazed plots.

Therefore, grazing and grazing exclusion were associated with different functional responses depending on whether functional change was measured as occupied trait space or as displacement in dominant trait composition relative to the baseline.

Supporting functional metrics are reported in the Supplementary Material (Fig. S4 and Supplementary Table S1). Rao's Q showed higher temporal variability in ungrazed plots, especially near the alpha-diversity scale. Functional dispersion showed weaker treatment separation and a less consistent pattern along the alpha–sampled-gamma accumulation profile. The standardised taxonomic–functional mismatch is retained as a supplementary diagnostic of whether functional temporal variability was higher, lower or similar to the corresponding taxonomic temporal variability (Fig. S5).

4.3. *Treatment contrasts along the alpha–gamma accumulation profile*

The signed treatment contrast summarised the direction and magnitude of differences between grazed and ungrazed communities along the rarefaction curve (Fig. 6). Positive values of ΔCV indicate higher temporal variability in ungrazed plots; negative values indicate higher temporal variability in grazed plots. Species richness, Shannon diversity and *CWM* displacement showed positive contrasts from the alpha-diversity scale to the sampled-gamma-diversity scale. Functional richness showed negative contrasts across the same gradient (Fig. 6; Table 1, Supplementary Table S1).

Contrasts in temporal trend showed a related but not identical pattern. Species richness and Shannon diversity had more negative slopes in ungrazed plots, indicating stronger taxonomic decline under grazing exclusion. Functional richness showed a positive slope in grazed

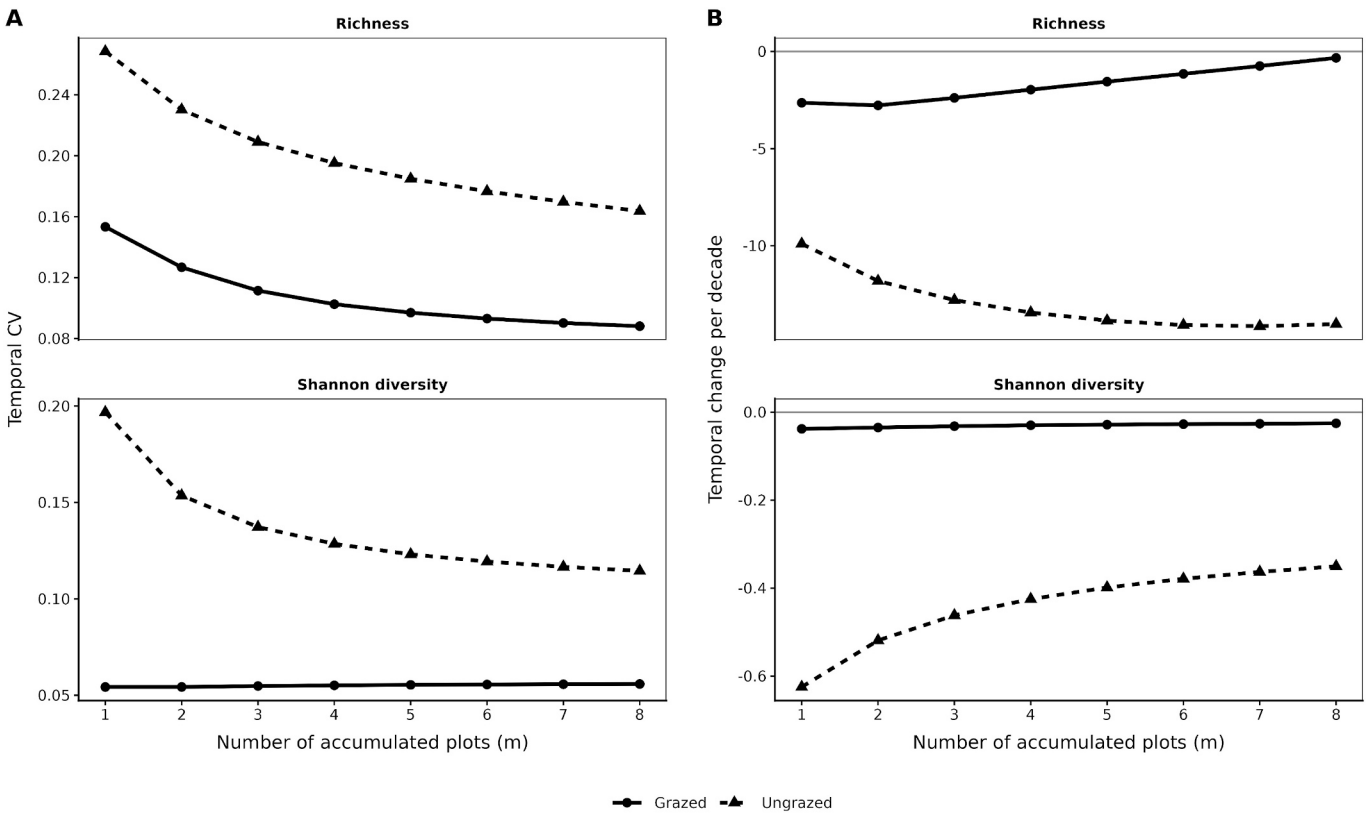


Fig. 4. Taxonomic temporal variability and trend profiles. Panel A shows the temporal coefficient of variation across survey-specific rarefaction curves at each number of accumulated plots. Panel B shows temporal change per decade estimated at each value of m. The trend profile makes the direction of temporal change explicit along the same rarefaction gradient used for the variability profile.

Table 1
Summary of temporal variability and temporal trend profiles for the main metrics. *AUC CV* is the discrete sum of temporal coefficient-of-variation values across the rarefaction gradient. *CV* at $m = 1$ represents temporal variability at the alpha-diversity scale, where diversity is evaluated for one plot.CV at m = N represents temporal variability for the complete pooled assemblage, corresponding to the sampled-gamma-diversity endpoint for diversity metrics. Temporal-change values are expressed per decade and describe the directional change in the expected rarefied value at $m = 1$ and $m = N$. The corresponding non-standardised *AUC SD* values are reported in the Supplementary Material. Values reported in Table 1 are point estimates. Bootstrap variance, standard errors and percentile 95% uncertainty intervals for the corresponding profiles, endpoint differences and whole-profile summaries are reported in Supplementary Tables S11–S14.

Metric	Treatment	*AUC CV*	*CV* at $m = 1$	*CV* at $m = N$	Temporal change at $m = 1$	Temporal change at $m = N$
Richness	Grazed	0.863	0.153	0.088	−2.641	−0.332
Richness	Ungrazed	1.598	0.268	0.164	−9.899	−14.025
Shannon diversity	Grazed	0.441	0.054	0.056	−0.038	−0.025
Shannon diversity	Ungrazed	1.090	0.197	0.114	−0.625	−0.350
Functional richness (*FRic*)	Grazed	0.700	0.128	0.078	−0.014	0.669
Functional richness (*FRic*)	Ungrazed	0.377	0.073	0.043	−0.741	−0.226
CWM displacement	Grazed	2.972	0.228	0.455	0.102	0.153
CWM displacement	Ungrazed	4.135	0.426	0.562	0.628	0.659

plots and a negative slope in ungrazed plots, indicating divergent temporal change in occupied dominant-species trait space. *CWM* displacement increased in both treatments but more strongly in ungrazed plots, showing greater directional movement away from the initial dominant trait composition under grazing exclusion.

At the level of point estimates, the treatment contrasts therefore revealed distinct patterns of temporal variability and directional change across taxonomic and functional descriptors. Ungrazed communities showed higher temporal variability in taxonomic diversity and in directional functional displacement. Grazed communities showed higher temporal variability in functional richness. Ungrazed communities also showed stronger directional taxonomic decline and stronger directional *CWM* displacement, whereas grazed communities showed a stronger positive temporal change in functional richness. These descriptive patterns were visible across the full alpha–sampled-gamma accumulation profile, but the strength of the contrast changed with the number of accumulated plots. The bootstrap analysis showed, however, that sampling support for these differences varied substantially among biodiversity metrics. The full rarefaction profile therefore retained information that would be lost if analyses were restricted to alpha- or sampled-gamma-diversity endpoints.

4.4. Sampling uncertainty

Sampling uncertainty was substantially lower relative to the observed treatment contrasts for the taxonomic metrics than for the functional metrics (Figs. S6–S8; Tables S11–S14). For species richness, the Ungrazed − Grazed difference in temporal CV had a percentile 95% uncertainty interval excluding zero from $m = 1$ to $m = 6$. For Shannon diversity, the temporal-*CV* contrast excluded zero at all eight

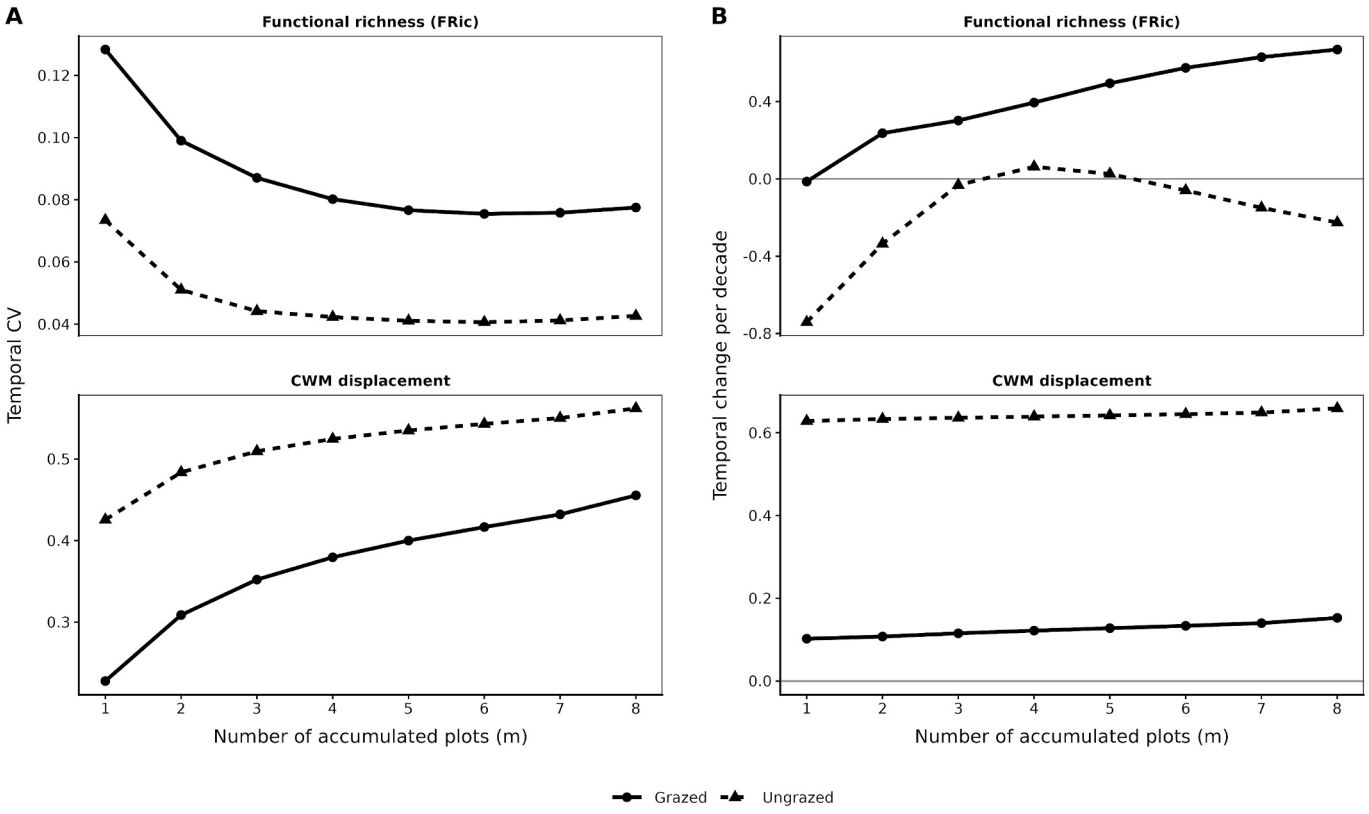


Fig. 5. Functional temporal variability and trend profiles for the main functional outputs. Functional richness was calculated as convex-hull area in the first two axes of the standardised trait ordination. *CWM* displacement is the Euclidean distance between the rarefied community-weighted mean trait vector and the first-year treatment-specific baseline. Panel A shows temporal *CV* and Panel B shows temporal change per decade.

accumulation levels. The difference in temporal change per decade excluded zero throughout the accumulation gradient for both richness and Shannon diversity, consistently indicating stronger taxonomic decline in ungrazed plots. Whole-profile temporal-*CV* contrasts were also supported for richness ($\Delta AUC = 0.735$, 95% interval = 0.062–1.428) and Shannon diversity ($\Delta AUC = 0.648$, 0.213–1.275).

The functional point-estimate profiles retained the directions described above, but their between-treatment uncertainty was greater. For functional richness, the 95% interval for the temporal-*CV* treatment contrast included zero at every accumulation level, as did the temporal-change contrast. For *CWM* displacement, the temporal-*CV* treatment contrast also included zero throughout the accumulation profile, while the temporal-change contrast excluded zero only at $m = 1$ and $m = 2$. The functional profiles should therefore be interpreted primarily as descriptive differences in this worked example rather than as equally well-supported treatment effects across the accumulation gradient.

Direct comparison of the endpoints showed that richness temporal *CV* decreased from $m = 1$ to $m = N$ in both grazing treatments, with 95% uncertainty intervals excluding zero. Shannon *CV* decreased from $m = 1$ to $m = N$ in ungrazed plots but not in grazed plots. In contrast, *CWM*-displacement *CV* increased from $m = 1$ to $m = N$ in both treatments. The block-aware analysis also indicated a decline in functional-richness *CV* in grazed plots, although this result was borderline under the alternative permanent-plot bootstrap and was therefore not considered a robust endpoint difference.

The alternative treatment-wise permanent-plot bootstrap produced essentially the same uncertainty structure as the primary block-aware procedure (Table S15). Standard errors of the treatment contrasts were highly correlated between the two analyses (r = 0.995), and their mean 95% interval widths were virtually identical (ratio = 0.9995). The few differences in whether individual intervals narrowly crossed zero were restricted to borderline accumulation levels and did not change the overall interpretation.

4.5. Null expectations

The random species-allocation null showed that accumulation-dependent richness patterns were treatment dependent (Fig. S9; Tables S16–S16C). In grazed plots, neither the temporal-*CV* profile nor the temporal-change profile differed globally from the random-allocation expectation (global $p = 0.1728$ and $p = 0.5412$, respectively). The observed reduction in temporal *CV* between $m = 1$ and $m = N$ (−0.0652) was also consistent with the null distribution (null mean = −0.0534, $p = 0.0892$).

In ungrazed plots, the richness temporal-*CV* profile differed from the random-allocation expectation (global $p = 0.0338$). Temporal *CV* decreased from 0.268 at $m = 1$ to 0.164 at $m = N$, and the corresponding endpoint difference (−0.1048) was more negative than expected under random species allocation (null mean = −0.0850, $p = 0.012$). The temporal-change profile also differed strongly from the null expectation (global $p = 0.0008$), with the largest departures occurring at low-to-intermediate accumulation levels. Thus, the observed accumulation-dependent richness structure under grazing exclusion could not be reproduced completely by random allocation of species among plots conditional on annual plot richness and species commonness.

The exact within-block grazing-label randomisation provided stronger evidence for the taxonomic treatment contrasts (Fig. S10; Tables S17–S17C). For both richness and Shannon diversity, the observed Ungrazed − Grazed differences in temporal *CV* and temporal change fell outside the 95% null envelopes at every value of *m*. Global randomisation tests rejected the label-exchangeability null for richness temporal *CV* ($p = 0.00463$), richness temporal change ($p = 0.00154$), Shannon temporal *CV* ($p = 0.00309$) and Shannon temporal change

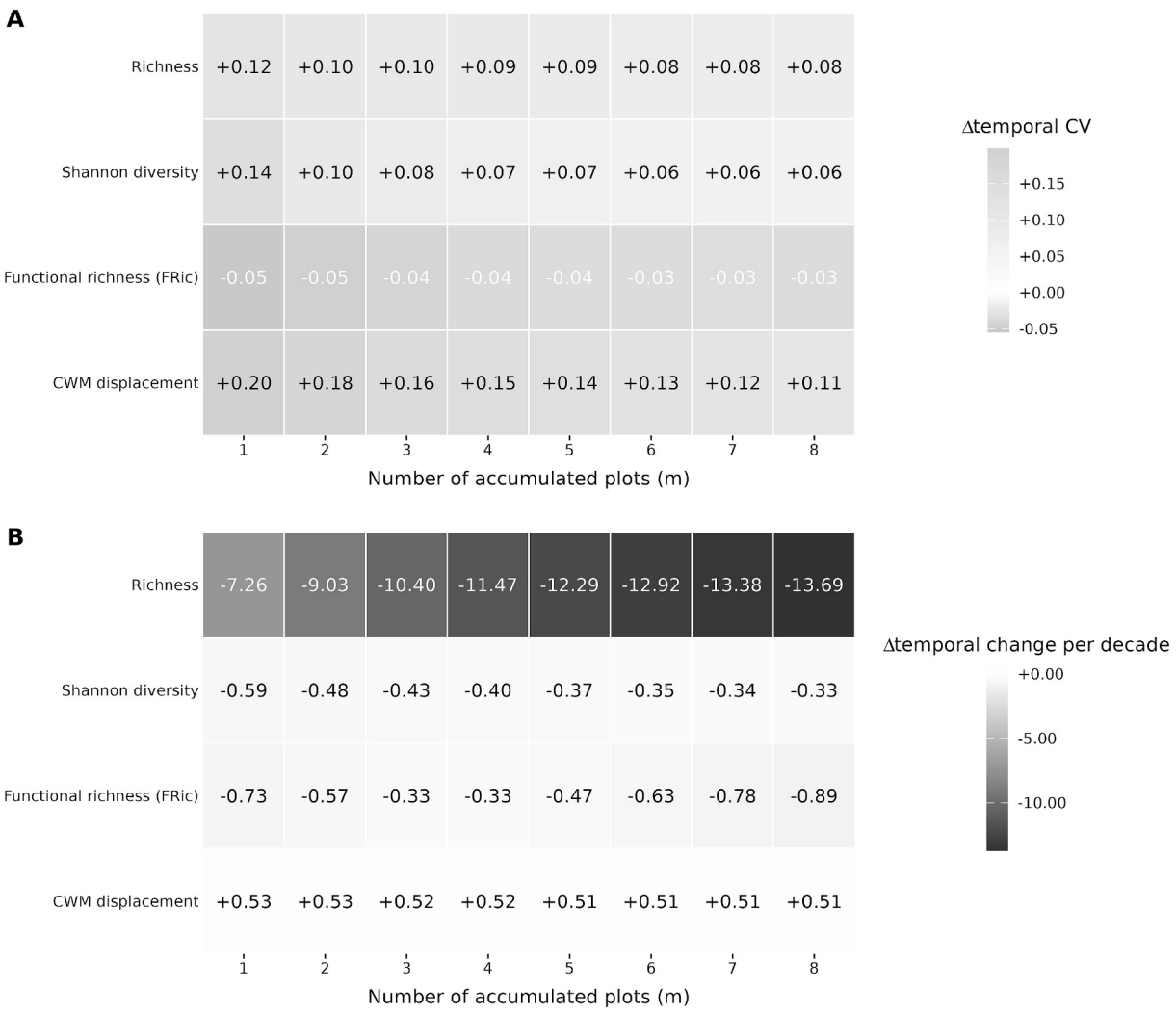


Fig. 6. Treatment contrasts in temporal variability and temporal trend along the alpha-sampled-gamma accumulation gradient. Panel A reports Δ temporal $CV = CV_ungrazed - CV_grazed$. Panel B reports Δ temporal change per decade = temporal change_ungrazed − temporal change_grazed. Positive values indicate higher values in ungrazed plots; negative values indicate higher values in grazed plots. Values shown here are point-estimate treatment contrasts. Corresponding resampling-based 95% uncertainty intervals are shown in Fig. S7 and reported numerically in Table S12.

($p = 0.00617$). Whole-profile *AUC* contrasts were likewise outside the exact null distributions for both metrics and both temporal descriptors (all $p \leq 0.00463$).

4.6. Trait coverage and robustness checks

Trait coverage was sufficient for the functional analyses but varied among years and treatments (Fig. S11 and Supplementary Table S1). The lowest coverage occurred in grazed plots in 2007, where one plot had markedly low trait-covered abundance. After applying the plot-year filter, six of eight grazed plots were retained in 2007 and all plots were retained in the remaining treatment-years(Supplementary Table S1).

Sensitivity analyses retained the direction of the point-estimate functional contrasts (Fig. S12). Increasing the minimum pooled trait-cover threshold from 0.50 to 0.60 and 0.70 did not change the direction of the functional results. The plot-year filter produced the same qualitative pattern: *CWM* displacement remained more temporally variable in ungrazed plots, whereas functional richness remained more temporally variable in grazed plots. Thus, the direction of the functional profiles was robust to variation in trait coverage and was not driven by the low-coverage grazed plot-years in 2007. This robustness to trait-data decisions should, however, be distinguished from sampling uncertainty in the between-treatment contrasts, which was substantially greater for functional than for taxonomic metrics (Fig. S7).

5. Discussion

Rarefaction profiles for repeated surveys complement species–time relationships and temporal beta-diversity analyses (Adler and Lauenroth, 2003; Magurran et al., 2019; Preston, 1960). They neither accumulate species through time nor decompose compositional turnover; instead, they identify where temporal variability and directional change are expressed along sampling-unit accumulation. In the Monte Labbro example, the taxonomic treatment contrast in temporal variability was strongest towards low values of m, whereas functional richness and *CWM* displacement captured changes in trait-space extent and centroid position, respectively. The example did not show a reversal in the direction of temporal change between $m = 1$ and $m = N$, nor is it intended to exemplify every idealised diagnostic pattern; rather, it demonstrates how the magnitude and sampling support of temporal differences can vary continuously along the accumulation gradient.

The treatment contrasts further illustrate why taxonomic and functional profiles should be interpreted together. At Monte Labbro, grazing and grazing exclusion represent contrasting post-restoration trajectories

after shrub cutting in a formerly encroached calcareous grassland (Maccherini et al., 2007; Pavanetto et al., 2025). The greater taxonomic variability and stronger decline observed under exclusion are consistent with spatially heterogeneous vegetation reorganisation, in which colonisation, persistence and local dominance may differ among plots once repeated herbivory is removed. Previous analyses of the same experiment also showed that grazing and climatic extremes jointly influenced functional composition, with grazed vegetation showing stronger reorganisation during prolonged drought, whereas ungrazed vegetation retained more conservative strategies and comparatively stable functional richness (Pavanetto et al., 2025). This context is compatible with the higher point-estimate variability of functional richness in grazed plots. Conversely, greater *CWM* displacement in ungrazed plots can coexist with relatively stable functional richness because the dominant trait centroid may shift while the total extent of occupied trait space changes little. These interpretations remain hypotheses because the present profiles did not directly test competition, succession, shrub re-encroachment, weather effects or species turnover.

The null analyses sharpen the ecological interpretation of these profiles. The exact within-block label randomisation showed that the taxonomic differences between grazed and ungrazed plots were not a generic consequence of partitioning the permanent plots into two balanced groups. Both the magnitude of temporal variability and the stronger taxonomic decline in ungrazed plots were more extreme than expected under treatment-label exchangeability throughout the accumulation profile. This result provides formal support for an association between grazing status and the taxonomic temporal trajectories while retaining the original blocked design.

By contrast, the random species-allocation null showed why the shape of a temporal rarefaction profile should not itself be equated with a specific ecological process. In grazed plots, the observed decline in richness *CV* with increasing m was compatible with random allocation of species among plots once local richness and species commonness were retained. Thus, a decreasing variability profile is not sufficient evidence for spatial compensation or asynchronous dynamics. In ungrazed plots, however, the decline in richness *CV* was stronger than expected under random allocation and the complete temporal-change profile also departed from the null expectation. This indicates that non-random among-plot species organisation contributes to the observed accumulation-dependent response under grazing exclusion. The null model does not identify the underlying mechanism, and processes such as spatially structured occupancy, differential colonisation or extinction, or compensatory dynamics therefore remain possible rather than uniquely demonstrated interpretations.

The temporal-change profiles added a further distinction: taxonomic diversity declined more strongly in ungrazed plots, functional richness showed a more positive trajectory in grazed plots, and *CWM* displacement increased more strongly in ungrazed plots. The uncertainty analysis showed, however, that these patterns were not equally well supported. Taxonomic treatment contrasts, particularly for Shannon diversity and temporal change in richness, were supported across most or all of the accumulation gradient. In contrast, the functional-richness treatment contrasts and the temporal-*CV* contrast for *CWM* displacement had uncertainty intervals overlapping zero throughout the profile. These functional results are therefore more appropriately interpreted as descriptive tendencies in the worked example rather than as strong evidence of grazing effects.

For monitoring design, the main value of the framework is that it links the interpretation of temporal change to the level of sampling-unit accumulation.A declining temporal-*CV* profile indicates that temporal variability decreases relative to the mean as sampling units are pooled; an increasing profile indicates that relative temporal variability becomes more pronounced at higher accumulation levels; and a consistently high profile indicates that relative temporal variability remains substantial across the accumulation gradient. The trend profile similarly identifies where directional increase or decline is strongest. These patterns describe the behaviour of biodiversity with increasing aggregation of sampling units; they should not be interpreted as changes across spatial grain or extent unless the spatial configuration of the sampling design is incorporated explicitly. Grain, focus and extent nevertheless remain important properties of the sampling design and influence the ecological interpretation of biodiversity change (Chase et al., 2018; Levin, 1992; Scheiner et al., 2011).

Several limitations should be considered. First, temporal rarefaction profiles require comparable sampling units repeatedly surveyed through time. Permanent plots or consistently revisited sampling units are ideal. There is no universal physical size for a sampling unit, but units compared within an analysis should have a consistent area, survey protocol and ecological meaning. The $m = 1$ endpoint inherits the observational grain of one unit, whereas $m = N$ represents the complete set of sampled units rather than landscape-scale gamma diversity. The number of sampling units determines both the maximum m and the resolution of the profile. Thus, a design with $N = 8$, as in each treatment here, can be analysed but provides only eight accumulation levels and limited spatial replication; explicit uncertainty estimates are therefore essential, and sensitivity to the chosen spatial resampling unit should be evaluated when alternative units are defensible. When groups or survey occasions contain different numbers of units, comparisons should be restricted to a common range of m, standardised by sample coverage, or based on a clearly defined resampling scheme. There is likewise no universal minimum number of survey occasions, because adequacy depends on the metric, temporal structure and inferential objective. Very short series nevertheless yield unstable estimates of temporal dispersion and trend and provide little basis for assessing departures from linear change; temporal uncertainty should therefore be quantified and conclusions kept descriptive. The present example includes 16 survey occasions between 2001 and 2019, providing relatively strong temporal replication despite the limited number of plots per treatment. A related limitation concerns imperfect detection. Spatial and temporal variation in observed diversity and species occurrence may arise from variation in detectability, in addition to or instead of actual ecological change. Detectability can vary with life-history stage, season, population density, survey effort, observer and time of day (Alexander et al., 2009; Bacaro and Fonda, 2026; Watson, 2010). Unless detectability is modelled separately, the profiles should therefore be interpreted as describing temporal patterns in the recorded data, which may combine variation in true occurrence and detection. For a focal species known independently to occur at a site, however, a potential extension would be to use the framework to quantify how detection varies through time and along the sampling-unit accumulation curve. Such an application would complement rather than replace occupancy or mark–recapture models that explicitly estimate detection probability.

Second, temporal variability and temporal trend profiles describe different aspects of change and should not be conflated. A high temporal *CV* can result from a monotonic trend, cyclic variation, episodic disturbance or irregular interannual fluctuation. *CV* also expresses temporal dispersion relative to the temporal mean and can become unstable when that mean approaches zero; it should therefore not be interpreted as a universally sufficient measure of temporal variability or stability (Chao et al., 2025). The sensitivity analysis performed here illustrates this distinction. Information-based variability at $q = 1$ retained the principal treatment contrasts and closely reproduced the shape of the *CV* profiles, while $q = 2$ showed the expected strong correspondence with *CV*-based variability. Non-standardised temporal *SD* also retained the direction of all main treatment contrasts, but its profile did not always have the same shape. For species richness, in particular, absolute *SD* increased with sampling-unit accumulation while relative *CV* decreased because mean accumulated richness increased strongly along the curve. Thus, absolute temporal dispersion and variability relative to the temporal mean are complementary rather than interchangeable descriptions of temporal change.

The trend profile addresses part of this ambiguity by estimating the

direction of change at each level of accumulation, but it remains a descriptive profile of linear change along the rarefaction curve. Strict stationarity is not a prerequisite for calculating this descriptive profile, and using the actual calendar years accommodates irregular survey intervals. However, this neither recovers information for unsurveyed years nor captures marked non-stationarity. Complementary nonlinear, change-point, temporal-autocorrelation-aware or temporal null models are still needed when the timing of disturbance or formal inference on temporal structure is the primary question.

Third, the interpretation depends on the metric being rarefied. Richness, Shannon diversity, functional richness, Rao's *Q*, functional dispersion and *CWM* displacement have different numerical behaviour and different ecological meanings. Temporal rarefaction profiles should therefore be interpreted with reference to the ecological quantity being accumulated.

Functional applications require additional care. In the worked example, functional rarefaction was based on a fixed trait matrix for the dominant trait-covered species subset. The functional profiles therefore describe how species composition and abundance change within a fixed trait space. They do not measure annual intraspecific trait variation or trait plasticity. This distinction is important because intraspecific trait variability can alter functional diversity estimates and community trait responses, especially in plant communities exposed to environmental gradients, grazing or disturbance (Albert et al., 2010; Siefert et al., 2015; Violle et al., 2012). *CWM* displacement also depends on the selected baseline. A first-year baseline is appropriate when the objective is to describe departure from the initial observed state, but other baselines may be preferable for restoration targets, reference communities or experimental controls. *CWM* displacement should therefore be reported as directional functional reorganisation, not as functional diversity. The same caution applies to its trend profile: a positive slope indicates increasing departure from the selected baseline, not an increase in functional diversity.

Sampling uncertainty should also be distinguished from the temporal variability represented by the profile itself. In the worked example, resampling both the spatial sampling units and the observed survey occasions propagated finite-sample uncertainty to temporal *CV*, temporal change, *AUC* summaries and treatment contrasts. The primary block-aware procedure retained the experimental layout and repeated-measures structure, while a sensitivity analysis based on permanent plots within grazing groups produced nearly identical uncertainty estimates. More generally, the appropriate spatial resampling unit should follow the dependence and sampling structure of the monitoring design. Because the present experiment contains only four blocks, the bootstrap intervals should be interpreted as resampling-based uncertainty estimates rather than as a substitute for a full mixed-effects or autocorrelation-aware time-series model.

The framework can be extended in several directions. Coverage-based temporal rarefaction would allow comparisons among years, sites or treatments that differ in sample completeness, following the logic of coverage standardisation in diversity estimation (Chao et al., 2014; Chao and Jost, 2012). Spatially constrained temporal rarefaction could be used when permanent plots are spatially ordered, clustered or autocorrelated, by constructing annual curves from spatially constrained rather than fully random subsets (Bacaro et al., 2016; Chiarucci et al., 2009).

The null models used here address two specific reference processes: random allocation of species among sampling units and exchangeability of grazing labels under the blocked experimental design. Other null formulations could be developed for different ecological questions. For example, year-label permutations, cyclic shifts or constrained temporal permutations could be used when the hypothesis concerns temporal exchangeability, autocorrelation or the timing of disturbances. Null-model choice should therefore follow the ecological hypothesis and dependence structure of the monitoring design rather than being treated as a generic component of the rarefaction procedure. Such extensions retain the same rarefaction structure while allowing descriptive profiles to be embedded in explicit hypothesis tests when appropriate.

Analytical reproducibility is also important, although the primary contribution of the framework is ecological rather than software-oriented. Implementing the temporal workflow within *Rarefy* or a compatible reproducible framework would extend its existing taxonomic, functional, phylogenetic and spatially explicit rarefaction tools to repeated surveys and provide standardised outputs for annual curves, temporal profiles and treatment contrasts (Thouverai et al., 2026).

Rarefaction profiles for repeated biodiversity surveys add an accumulation-explicit diagnostic tool to long-term biodiversity monitoring. They do not replace rarefaction endpoints, temporal beta diversity, trend models or compositional analyses. Their contribution is to show whether temporal variability and directional change are associated mainly with expected alpha diversity, with sampled gamma diversity, or with the accumulation from alpha to sampled gamma. This information is useful when monitoring aims not only to detect that communities have changed, but also to identify the level of sampling-unit accumulation and the biodiversity dimension at which temporal change is most clearly expressed.

Data accessibility and code availability

The community and trait data used in this manuscript derive from the Monte Labbro long-term vegetation experiment and the associated trait dataset described by Pavanetto et al. (2025). The cleaned community matrix, harmonised trait table, analysis-ready input files, derived output tables, figure data and *R* scripts used to reproduce all analyses and figures are available through Figshare and GitHub. The Figshare archive provides the stable release of the data and analysis outputs, including the rarefaction outputs, temporal variability profiles, temporal trend profiles, summary tables and underlying data used to generate the figures. The GitHub repository hosts the reproducible analytical workflow used for data preparation, temporal rarefaction analysis, trend-profile estimation, robustness checks and figure/table production. The repository also includes the stand-alone *temporal_rarefy()* development function used in this study, which is intended to support reproducible application of the framework to repeated biodiversity surveys.

Figshare repository: https://figshare.com/s/63166078e4776aebe8e8

GitHub repository: https://github.com/gbacaro/Rarefy_advanced

CRediT authorship contribution statement

Giovanni Bacaro: Writing – review & editing, Writing – original draft, Software, Investigation, Formal analysis, Conceptualization. **Emanuele Fanfarillo:** Investigation, Data curation. **Simona Maccherini:** Project administration, Data curation, Conceptualization.

Funding

This research received no external funding. No specific grant from any funding agency in the public, commercial or not-for-profit sectors supported the development of this manuscript.

Declaration of competing interest

The authors declare that they have no known competing financial interests or personal relationships that could have appeared to influence the work reported in this paper.

Appendix A. Supplementary data

Supplementary data to this article can be found online at https://doi.org/10.1016/j.ecoinf.2026.104113.

Data availability

Data and code are available on GitHub

References

Adler, P.B., Lauenroth, W.K., 2003. The power of time: spatiotemporal scaling of species diversity. Ecol. Lett. 6, 749–756. https://doi.org/10.1046/j.1461-0248.2003.00497.x.

Adler, P.B., White, E.P., Lauenroth, W.K., Kaufman, D.M., Rassweiler, A., Rusak, J.A., 2005. Evidence for a general species-time-area relationship. Ecology 86, 2032–2039. https://doi.org/10.1890/05-0067.

Albert, C.H., Thuiller, W., Yoccoz, N.G., Soudant, A., Boucher, F., Saccone, P., Lavorel, S., 2010. Intraspecific functional variability: extent, structure and sources of variation. J. Ecol. 98, 604–613. https://doi.org/10.1111/j.1365-2745.2010.01651.x.

Alexander, H.M., Slade, N.A., Kettle, W.D., Pittman, G.L., Reed, A.W., 2009. Detection, survival rates and dynamics of a cryptic plant, *Asclepias meadii*: applications of mark-recapture models to long-term monitoring studies. J. Ecol. 97, 267–276. https://doi.org/10.1111/j.1365-2745.2008.01468.x.

Bacaro, G., 2026. Shades of gray: a continuum of biodiversity understanding from dark to bright diversity. Ecol. Diversity 2 (4), 10012. https://doi.org/10.70322/ecoldivers.2025.10012.

Bacaro, G., Altobelli, A., Cameletti, M., Ciccarelli, D., Martellos, S., Palmer, M.W., Ricotta, C., Rocchini, D., Scheiner, S.M., Tordoni, E., Chiarucci, A., 2016. Incorporating spatial autocorrelation in rarefaction methods: implications for ecologists and conservation biologists. Ecol. Indic. 69, 233–238. https://doi.org/10.1016/j.ecolind.2016.04.026.

Bacaro, G., Baragatti, E., Chiarucci, A., 2009. Using taxonomic data to assess and monitor biodiversity: are the tribes still fighting? J. Environ. Monit. 11, 798–801. https://doi.org/10.1039/b818171n.

Bacaro, G., Fonda, F., 2026. Toward the full operationalization of the dark diversity concept in environmental impact assessments: a call to revise international EIA standards. Conserv. Lett. 19, e70034. https://doi.org/10.1111/con4.70034.

Bartlett, M.K., Scoffoni, C., Sack, L., 2012. The determinants of leaf turgor loss point and prediction of drought tolerance of species and biomes. Ecol. Lett. 15, 393–405. https://doi.org/10.1111/j.1461-0248.2012.01751.x.

Blowes, S.A., Supp, S.R., Antao, L.H., Bates, A., Bruelheide, H., Chase, J.M., Moyes, F., Magurran, A.E., McGill, B.J., Myers-Smith, I.H., Winter, M., Bjorkman, A.D., Bowler, D.E., Byrnes, J.E.K., Gonzalez, A., Hines, J., Isbell, F., Jones, H.P., Navarro, L.M., Thompson, P.L., Vellend, M., Waldock, C., Dornelas, M., 2019. The geography of biodiversity change in marine and terrestrial assemblages. Science 366, 339–345. https://doi.org/10.1126/science.aaw1620.

Carmona, C.P., de Bello, F., Mason, N.W.H., Lepš, J., 2016. Traits without borders: integrating functional diversity across scales. Trends Ecol. Evol. 31, 382–394. https://doi.org/10.1016/j.tree.2016.02.003.

Chao, A., Colwell, R.K., Shia, J., Thorn, S., Yang, M.-Y., Mitesser, O., Huang, Y.-T., Kortmann, M., Mori, A.S., Delory, B.M., Fichtner, A., Huang, Y., Roscher, C., Schmid, B., Eisenhauer, N., Müller, J., 2025. A continuum of information-based temporal stability measures and their decomposition across hierarchical levels. bioRxiv. https://doi.org/10.1101/2025.08.20.671203.

Chao, A., Gotelli, N.J., Hsieh, T.C., Sander, E.L., Ma, K.H., Colwell, R.K., Ellison, A.M., 2014. Rarefaction and extrapolation with hill numbers: a framework for sampling and estimation in species diversity studies. Ecol. Monogr. 84, 45–67. https://doi.org/10.1890/13-0133.1.

Chao, A., Jost, L., 2012. Coverage-based rarefaction and extrapolation: standardizing samples by completeness rather than size. Ecology 93, 2533–2547. https://doi.org/10.1890/11-1952.1.

Chao, A., Thorn, S., Chiu, C.-H., Moyes, F., Hu, K.-H., Chazdon, R.L., Wu, J., Magnago, L.F.S., Dornelas, M., Zelený, D., Colwell, R.K., Magurran, A.E., 2023. Rarefaction and extrapolation with beta diversity under a framework of Hill numbers: the iNEXT.beta3D standardisation. Ecol. Monogr. 93, e1588. https://doi.org/10.1002/ecm.1588.

Chase, J.M., McGill, B.J., McGlinn, D.J., May, F., Blowes, S.A., Xiao, X., Knight, T.M., Purschke, O., Gotelli, N.J., 2018. Embracing scale-dependence to achieve a deeper understanding of biodiversity and its change across communities. Ecol. Lett. 21, 1737–1751. https://doi.org/10.1111/ele.13151.

Chiarucci, A., Bacaro, G., Rocchini, D., Fattorini, L., 2008. Discovering and rediscovering the sample-based rarefaction formula in the ecological literature. Community Ecol. 9, 121–123. https://doi.org/10.1556/ComEc.9.2008.1.14.

Chiarucci, A., Bacaro, G., Rocchini, D., Ricotta, C., Palmer, M.W., Scheiner, S.M., 2009. Spatially constrained rarefaction: incorporating the autocorrelated structure of biological communities into sample-based rarefaction. Community Ecol. 10, 209–214. https://doi.org/10.1556/ComEc.10.2009.2.11.

Colwell, R.K., Mao, C.X., Chang, J., 2004. Interpolating, extrapolating, and comparing incidence-based species accumulation curves. Ecology 85, 2717–2727. https://doi.org/10.1890/03-0557.

Díaz, S., Kattge, J., Cornelissen, J.H.C., Wright, I.J., Lavorel, S., Dray, S., Reu, B., et al., 2016. The global spectrum of plant form and function. Nature 529, 167–171. https://doi.org/10.1038/nature16489.

Dornelas, M., Gotelli, N.J., McGill, B.J., Shimadzu, H., Moyes, F., Sievers, C., Magurran, A.E., 2014. Assemblage time series reveal biodiversity change but not systematic loss. Science 344, 296–299. https://doi.org/10.1126/science.1248484.

Gotelli, N.J., Colwell, R.K., 2001. Quantifying biodiversity: procedures and pitfalls in the measurement and comparison of species richness. Ecol. Lett. 4, 379–391. https://doi.org/10.1046/j.1461-0248.2001.00230.x.

Hillebrand, H., Blasius, B., Borer, E.T., Chase, J.M., Downing, J.A., Eriksson, B.K., Filstrup, C.T., Harpole, W.S., Hodapp, D., Larsen, S., Lewandowska, A.M., Seabloom, E.W., Van de Waal, D.B., Ryabov, A.B., 2018. Biodiversity change is uncoupled from species richness trends: consequences for conservation and monitoring. J. Appl. Ecol. 55, 169–184. https://doi.org/10.1111/1365-2664.12959.

Laliberté, E., Legendre, P., 2010. A distance-based framework for measuring functional diversity from multiple traits. Ecology 91, 299–305. https://doi.org/10.1890/08-2244.1.

Lavorel, S., Garnier, E., 2002. Predicting changes in community composition and ecosystem functioning from plant traits: revisiting the Holy Grail. Funct. Ecol. 16, 545–556. https://doi.org/10.1046/j.1365-2435.2002.00664.x.

Levin, S.A., 1992. The problem of pattern and scale in ecology. Ecology 73, 1943–1967. https://doi.org/10.2307/1941447.

Maccherini, S., Bacaro, G., Favilli, L., Piazzini, S., Santi, E., Marignani, M., 2009. Congruence among vascular plants and butterflies in the evaluation of grassland restoration success. Acta Oecol. 35, 311–317. https://doi.org/10.1016/j.actao.2008.12.002.

Maccherini, S., Marignani, M., Castagnini, P., van den Brink, P.J., 2007. Multivariate analysis of the response of overgrown semi-natural calcareous grasslands to restorative shrub cutting. Basic Appl. Ecol. 8, 332–342. https://doi.org/10.1016/j.baae.2006.06.002.

Magurran, A.E., Dornelas, M., Moyes, F., Henderson, P.A., Storch, D., 2019. Temporal beta diversity: a macroecological perspective. Glob. Ecol. Biogeogr. 28, 1949–1960. https://doi.org/10.1111/geb.13026.

Mason, N.W.H., Mouillot, D., Lee, W.G., Wilson, J.B., 2005. Functional richness, functional evenness and functional divergence: the primary components of functional diversity. Oikos 111, 112–118. https://doi.org/10.1111/j.0030-1299.2005.13886.x.

McGill, B.J., Enquist, B.J., Weiher, E., Westoby, M., 2006. Rebuilding community ecology from functional traits. Trends Ecol. Evol. 21, 178–185. https://doi.org/10.1016/j.tree.2006.02.002.

Pavanetto, N., Tordoni, E., Petruzzellis, F., Maccherini, S., Nardini, A., Beccari, E., Ricotta, C., Rocchini, D., Conti, L., Fanfarillo, E., Castello, M., Bacaro, G., 2025. Effect of climate extremes and grazing on functional traits of a grassland community: insights from a 20-year experiment. Ann. Bot. 136, 129–139. https://doi.org/10.1093/aob/mcaf059.

Pavoine, S., 2020. adiv: an R package to analyse biodiversity in ecology. Methods Ecol. Evol. 11, 1106–1112. https://doi.org/10.1111/2041-210X.13430.

Pavoine, S., Ricotta, C., 2014. Functional and phylogenetic similarity among communities. Methods Ecol. Evol. 5, 666–675. https://doi.org/10.1111/2041-210X.12193.

Preston, F.W., 1960. Time and space and the variation of species. Ecology 41, 611–627. https://doi.org/10.2307/1931793.

R Core Team, 2026. R: A Language and Environment for Statistical Computing. R Foundation for Statistical Computing, Vienna, Austria. https://www.R-project.org/.

Rao, C.R., 1982. Diversity and dissimilarity coefficients: a unified approach. Theor. Popul. Biol. 21, 24–43. https://doi.org/10.1016/0040-5809(82)90004-1.

Reich, P.B., 2014. The world-wide 'fast–slow' plant economics spectrum: a traits manifesto. J. Ecol. 102, 275–301. https://doi.org/10.1111/1365-2745.12211.

Ricotta, C., Acosta, A.T.R., Bacaro, G., Carboni, M., Chiarucci, A., Rocchini, D., Pavoine, S., 2019. Rarefaction of beta diversity. Ecol. Indic. 107, 105606. https://doi.org/10.1016/j.ecolind.2019.105606.

Ricotta, C., Pavoine, S., Bacaro, G., Acosta, A.T.R., 2012. Functional rarefaction for species abundance data. Methods Ecol. Evol. 3, 519–525. https://doi.org/10.1111/j.2041-210X.2011.00178.x.

Rosenzweig, M.L., 1995. Species Diversity in Space and Time. Cambridge University Press.

Scheiner, S.M., 2003. Six types of species-area curves. Glob. Ecol. Biogeogr. 12, 441–447. https://doi.org/10.1046/j.1466-822X.2003.00061.x.

Scheiner, S.M., Chiarucci, A., Fox, G.A., Helmus, M.R., McGlinn, D.J., Willig, M.R., 2011. The underpinnings of the relationship of species richness with space and time. Ecol. Monogr. 81, 195–213. https://doi.org/10.1890/10-0985.1.

Shimadzu, H., Dornelas, M., Magurran, A.E., 2015. Measuring temporal turnover in ecological communities. Methods Ecol. Evol. 6, 1384–1394. https://doi.org/10.1111/2041-210X.12438.

Shinozaki, K., 1963. Note on the species area curve. In: Proceedings of the 10th Annual Meeting of the Ecological Society of Japan, pp. 1–5 (in Japanese).

Siefert, A., Violle, C., Chalmandrier, L., Albert, C.H., Taudiere, A., Fajardo, A., Aarssen, L.W., Baraloto, C., Carlucci, M.B., Cianciaruso, M.V., de Dantas, V.L., de Bello, F., Duarte, L.D.S., Fonseca, C.R., Freschet, G.T., Gaucherand, S., Gross, N., Hikosaka, K., Jackson, B., et al., 2015. A global meta-analysis of the relative extent of intraspecific trait variation in plant communities. Ecol. Lett. 18, 1406–1419. https://doi.org/10.1111/ele.12508.

Thouverai, E., Pavoine, S., Tordoni, E., Chiarucci, A., Ricotta, C., Rocchini, D., Bacaro, G., 2026. Rarefy: an R package for the calculation of taxonomic, functional and phylogenetic sample-based spatially explicit rarefaction curves. Ecol. Inform. 96, 103803. https://doi.org/10.1016/j.ecoinf.2026.103803.

Tuomisto, H., 2010a. A diversity of beta diversities: straightening up a concept gone awry. Part 1. Defining beta diversity as a function of alpha and gamma diversity. Ecography 33, 2–22. https://doi.org/10.1111/j.1600-0587.2009.05880.x.

Tuomisto, H., 2010b. A diversity of beta diversities: straightening up a concept gone awry. Part 2. Quantifying beta diversity and related phenomena. Ecography 33, 23–45. https://doi.org/10.1111/j.1600-0587.2009.06148.x.

Villéger, S., Mason, N.W.H., Mouillot, D., 2008. New multidimensional functional diversity indices for a multifaceted framework in functional ecology. Ecology 89, 2290–2301. https://doi.org/10.1890/07-1206.1.

Violle, C., Enquist, B.J., McGill, B.J., Jiang, L., Albert, C.H., Hulshof, C., Jung, V., Messier, J., 2012. The return of the variance: intraspecific variability in community ecology. Trends Ecol. Evol. 27, 244–252. https://doi.org/10.1016/j.tree.2011.11.014.

Violle, C., Navas, M.-L., Vile, D., Kazakou, E., Fortunel, C., Hummel, I., Garnier, E., 2007. Let the concept of trait be functional! Oikos 116, 882–892. https://doi.org/10.1111/j.0030-1299.2007.15559.x.

Watson, D.M., 2010. Optimizing inventories of diverse sites: insights from Barro Colorado Island birds. Methods Ecol. Evol. 1, 280–291. https://doi.org/10.1111/j.2041-210X.2010.00028.x.

White, E.P., Adler, P.B., Lauenroth, W.K., Gill, R.A., Greenberg, D., Kaufman, D.M., Rassweiler, A., Rusak, J.A., Smith, M.D., Steinbeck, J.R., Waide, R.B., Yao, J., 2006. A comparison of the species-time relationship across ecosystems and taxonomic groups. Oikos 112, 185–195. https://doi.org/10.1111/j.0030-1299.2006.14223.x.

Whittaker, R.H., 1960. Vegetation of the Siskiyou Mountains, Oregon and California. Ecol. Monogr. 30, 279–338. https://doi.org/10.2307/1943563.

Wickham, H., 2016. ggplot2: Elegant Graphics for Data Analysis. Springer-Verlag New York. https://doi.org/10.1007/978-3-319-24277-4.

Wright, I.J., Reich, P.B., Westoby, M., Ackerly, D.D., Baruch, Z., Bongers, F., Cavender-Bares, J., Chapin, T., Cornelissen, J.H.C., Diemer, M., Flexas, J., Garnier, E., Groom, P.K., Gulias, J., Hikosaka, K., Lamont, B.B., Lee, T., Lee, W., Lusk, C., et al., 2004. The worldwide leaf economics spectrum. Nature 428, 821–827. https://doi.org/10.1038/nature02403.

Yoccoz, N.G., Nichols, J.D., Boulinier, T., 2001. Monitoring of biological diversity in space and time. Trends Ecol. Evol. 16, 446–453. https://doi.org/10.1016/S0169-5347(01)02205-4.